Pergamon

Journal of Atmospheric and Solar-Terrestrial Physics, Vol. 59, No. 6, pp. 603–627, 1997

1364–6826/97 $17.00 + 0.00

PII: S0021–9169(96)00143–2

Intraseasonal wind variability in the equatorial mesosphere and lower thermosphere: long-term observations from the central Pacific

Stephen D. Eckermann,*†[1] Deepak K. Rajopadhyaya‡[2] and Robert A. Vincent[2]

[1]Computational Physics, Inc., 2750 Prosperity Avenue, Suite #600, Fairfax, VA 22031, U.S.A.;
[2]Department of Physics and Mathematical Physics, University of Adelaide, SA 5005, Australia

(*Received* 6 *August* 1996; *accepted* 9 *August* 1996)

Abstract—Analysis of intraseasonal (10–100 days) oscillations in the equatorial mesosphere and lower thermosphere (MLT) is presented, based on over five years of velocity data acquired by a radar system at Christmas Island (2°N, 157°W), in the central Pacific. Strong peaks in the zonal winds are found at periods of ~60 days, ~35–40 days, and ~22–25 days. These peaks, as well as the mean annual variations of the activity within the various period ranges, are similar to 30–60 day and 20–25 day oscillations that occur in the equatorial troposphere. Weaker (but nonetheless clear) periodicities are also found in the meridional winds at ~60 days and ~35 days. A strong quasi-60-day variation is detected in gravity-wave variances, with much weaker signals at ~40 days and ~25 days. Strong variations in diurnal tidal amplitudes are observed with periods of ~60 days, ~40 days, and ~25 days.

These observations lead us to propose the following explanation for the observed intraseasonal variability of the equatorial MLT region. Intraseasonal cycles in tropical tropospheric convection produce intraseasonal variations in the intensity of gravity waves and nonmigrating diurnal tides impinging upon the mesosphere. This accounts for the intraseasonal peaks we observe in gravity-wave and tidal activity. This intraseaonally modulated wave activity induces similar periodicities in the wave-induced driving of the zonal MLT flow, which in turn forces the observed intraseasonal peaks in the zonal MLT winds. If this explanation is valid, these observations provide an unusually clear example of the driving of MLT flow patterns by waves emanating from tropospheric systems, and highlight the importance of convectively generated waves in understanding the dynamics of the equatorial middle atmosphere.

INTRODUCTION

In recent years, high-quality long-term observations of the equatorial mesosphere and lower thermosphere (MLT) have increased our knowledge of this region considerably. Equatorial wind measurements from both the Upper Atmosphere Research Satellite (UARS) and ground-based radars have provided us with a detailed climatological picture of the mean circulation (e.g., Lieberman *et al*., 1993; Palo and Avery, 1993; Garcia *et al*., 1997), equatorial waves (e.g., Vincent, 1993; Canziani *et al*., 1995), normal modes (Wu *et al*., 1993; Harris and Vincent, 1993; Palo and Avery, 1996), tides (e.g., McLandress *et al*., 1996), and gravity waves (e.g., Isler and Fritts, 1996; Connor and Avery, 1996).

On analyzing radar winds from a mid-Pacific equatorial site, Eckermann and Vincent (1994) presented preliminary evidence of strong intraseasonal zonal-wind oscillations (periods ~10–100 days) at heights between about 80–98 km. They noted that this variability in many ways resembled intraseasonal oscillations encountered in the equatorial troposphere (Madden and Julian, 1994), but argued that the large-scale tropospheric wave disturbances associated with this activity could not propagate to mesospheric heights. However, since this intraseasonal activity modulates convective activity within the Indian and western Pacific regions (Hartmann and Gross, 1988; Dunkerton and Crum, 1995), Eckermann and Vincent (1994) hypothesized that a similar intraseasonal variation in the intensity of convectively generated gravity waves might result. If these waves propagated to mesospheric heights and dissipated, similar intra-

*Author to whom correspondence should be addressed: E. O. Hulburt Center for Space Research, Code 7641, Naval Research Laboratory, Washington, DC 20375, U.S.A. (e-mail: eckerman@ismap4.nrl.navy.mil; WWW: http://uap-www.nrl.navy.mil/dynamics/html/eckerman.html).

†Work performed at E. O. Hulburt Center for Space Research, Code 7641, Naval Research Laboratory, Washington, DC 20375, USA. (http://uap-www.nrl.navy.mil).

‡Now at CIRES, University of Colorado at Boulder, Boulder, CO 80309, USA. (http://cires.colorado edu).

Report Documentation Page

Form Approved
OMB No. 0704-0188

1. REPORT DATE	2. REPORT TYPE	3. DATES COVERED
AUG 1996		**00-00-1996 to 00-00-1996**

4. TITLE AND SUBTITLE	5a. CONTRACT NUMBER
Intraseasonal wind variability in the equatorial mesosphere and lower thermosphere: long-term observations from the central Pacific	5b. GRANT NUMBER
	5c. PROGRAM ELEMENT NUMBER
6. AUTHOR(S)	5d. PROJECT NUMBER
	5e. TASK NUMBER
	5f. WORK UNIT NUMBER
7. PERFORMING ORGANIZATION NAME(S) AND ADDRESS(ES) **Naval Research Laboratory,E.O. Hulburt Center for Space Research,Washington,DC,20375**	8. PERFORMING ORGANIZATION REPORT NUMBER
9. SPONSORING/MONITORING AGENCY NAME(S) AND ADDRESS(ES)	10. SPONSOR/MONITOR'S ACRONYM(S)
	11. SPONSOR/MONITOR'S REPORT NUMBER(S)

12. DISTRIBUTION/AVAILABILITY STATEMENT
Approved for public release; distribution unlimited

13. SUPPLEMENTARY NOTES

14. ABSTRACT
see report

15. SUBJECT TERMS

16. SECURITY CLASSIFICATION OF:			17. LIMITATION OF ABSTRACT	18. NUMBER OF PAGES	19a. NAME OF RESPONSIBLE PERSON
a. REPORT **unclassified**	b. ABSTRACT **unclassified**	c. THIS PAGE **unclassified**	**Same as Report (SAR)**	**25**	

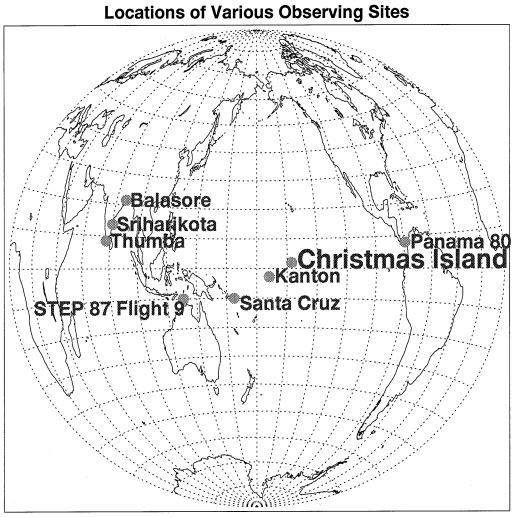

Fig. 1. Location of Christmas Island, as well as some other ground-based stations which provided data which we discuss later.

seasonal variability might then be transferred into the equatorial MLT flow.

The study of Eckermann and Vincent (1994), however, was preliminary. Its principal aim was to present a persuasive case for the existence of these oscillations, and to offer some possible explanations of their cause. Here, we investigate the intraseasonal activity in these data further, extending both the breadth of the analysis and the length of data analyzed. We also compute gravity-wave and tidal activities from higher-resolution wind data to investigate whether they correlate in any way with the intraseasonal wind variations, which might help to assess the gravity-wave-based theory for their generation suggested by Eckermann and Vincent (1994).

DATA

The wind data used in this study were acquired by a spaced antenna MF radar stationed at Christmas Island (2°N, 157°W), in the equatorial Pacific (see Fig. 1). The system measures horizontal wind velocities every 2 min at 2 km height intervals in the range 60–98 km (Vincent and Lesicar, 1991). The raw data were initially screened using an outlier-rejection algorithm, then diurnally averaged to give daily wind estimates at each height, as described by Eckermann and Vincent (1994). Eckermann and Vincent (1994) analyzed slightly less than 3 yr of data, obtained between 23 January, 1990 and 21 December, 1992 (1064 days), whereas here we incorporate data up to 21 May, 1995 (1944 days in all). These data provide us with nearly continuous time series of daily zonal and meridional winds, recorded at 2 km height intervals in the 60–98 km height range, which we use to study intraseasonal activity. Since diurnal data coverage below $\sim$75–80 km is incomplete, tidal effects may not be fully removed from the daily-averaged data at these lower heights, and so we focus mostly on the data above 80 km.

To study gravity-wave and tidal activity, we use higher-resolution time series which were formed by averaging the screened raw data into 4 min segments. These data extend to the end of 1994 only. Gravity-wave variances were computed by first band-passing the full 5 yr time series using a boxcar filter spanning the 12 min–4 h band, with missing data linearly interpolated. Thereafter, variances were computed by averaging the band-passed data over 2 day blocks, with interpolated regions excluded from the analysis. Modeling by Rastogi *et al.* (1996) indicates that horizontal-velocity variances at periods $\lesssim$ 1 h can be artificially enhanced by systematic instrumental effects. However, given the 'red' nature of wave frequency spectra, variances computed over the 12 min–4 h band are influenced more by the longer periods ($>$1 h) which are less affected by these biases (Rastogi *et al.*, 1996). Tidal structures were fitted using least-squares harmonic fits over a 6 day fitting window which was successively forwarded every 2 days. These procedures yielded time series of both gravity-wave variance and tidal amplitudes every 2 days for the full 5 yr of data.

SPECTRAL ANALYSIS

We begin by spectrally analyzing the velocity time series at a selected height, following and extending a similar preliminary analysis by Eckermann and Vincent (1994). Figure 2 profiles time series of zonal and meridional velocities at a height $z = 92$ km. The top row of plots shows the raw daily-averaged data, while the row below it shows the same data after smoothing with a 20 day running average.

Next, power spectral densities of the daily-averaged velocity time series were computed using numerical Fourier-transform methods. As in Eckermann and Vincent (1994), small gaps in the time series due to instrument downtime were interpolated prior to Fourier transformation using a cubic spline under tension. Resulting power spectral densities are plotted on the third row of Fig. 2 as a function of the harmonics of the fundamental frequency $\omega_f = (1944\,\text{days})^{-1}$: a corresponding period scale in days is shown on the upper axis for reference.

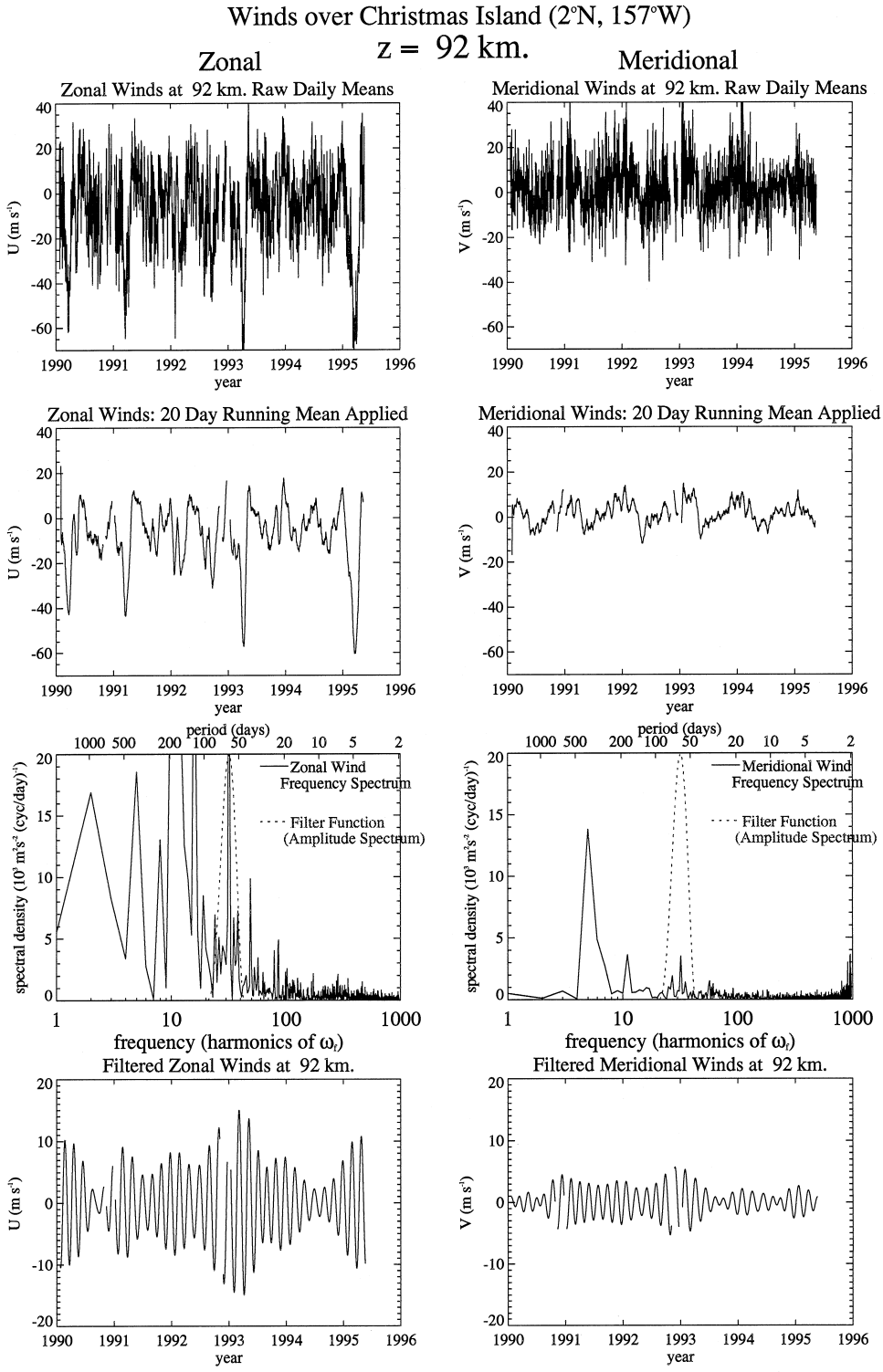

Fig. 2. Spectral analysis of time series at a height of 92 km of zonal (left column) and meridional (right column) velocities. The first row of plots shows the raw daily-averaged time series, which are then smoothed with a 20 day running average and plotted on the next row. Power spectra of the daily data are shown on the third row. A Hanning filter function is also shown with a dotted curve on these plots. It is used to band-pass fluctuations at $\sim$60 days. The resulting band-passed fluctuations are shown on the bottom row of plots.

These spectra show similar features to those computed from more-limited data by Eckermann and Vincent (1994). The zonal-velocity spectrum is dominated by a large off-scale peak at ~180 days due to the mesosphere and lower-thermosphere semiannual oscillation (MLTSAO), as well as smaller subsidiary peaks suggestive of slight annual (e.g., Vincent, 1993) and quasi-biennial influences. Additionally, as noted by Eckermann and Vincent (1994), there is rich structure in the spectrum within the 10–100 day period range: the so-called 'intraseasonal band.' Peaks near 60 days, 40 days, and 25 days are immediately evident.

The meridional velocity spectrum is dominated by a peak at ~360 days, produced by the annual variation of the global north–south circulation (Vincent, 1993). A smaller semiannual component is also evident here, which is absent at lower heights. Enhanced spectral power at ~2 days is produced by a strong quasi-2 day wave over Christmas Island (Harris and Vincent, 1993; Palo and Avery, 1996). However, in contrast to the earlier study of Eckermann and Vincent (1994) in which no clear intraseasonal peaks could be identified in the meridional velocities, the longer time series used here reveal small but distinct peaks in the meridional-velocity spectrum at ~60 days and ~35 days.

Since a peak near 60 days is common to the spectra of both velocity components in Fig. 2, we band-pass filter the amplitude spectra using a Hanning (cosine) filter which is centered near 60 days, as shown with a dotted curve on the spectral plots of Fig. 2. The resulting band-passed oscillations are plotted on the bottom row of Fig. 2.

Since 60 days is approximately the third harmonic of the strong MLTSAO peak at ~183 days, we must first ensure that this quasi-60 day zonal peak is not produced solely by higher harmonics of a nonsinusoidal MLTSAO. The 20 day running averages on the second row of Fig. 2 are particularly useful in assessing this. First, it is clear on inspecting these smoothed time series that the MLTSAO is strongly nonsinusoidal, and so will contribute higher harmonics. However, it is also clear that there are distinct intraseasonal oscillations in the smoothed zonal-velocity time series: see, for example, the two westward MLTSAO phases during 1992.

Our new finding here of similar (but smaller) oscillations in the meridional velocities confirms the reality of the quasi-60 day intraseasonal signals. The smoothed time series of meridional wind in Fig. 2 also shows clear intraseasonal 'wiggles,' this time superimposed upon a basic annual oscillation. Since the MLTSAO is, at best, extremely weak in the meridional winds, spectral leakage from a nonsinusoidal MLTSAO cannot explain the 60 day meridional peak observed here. Note too that the band-passed oscillations of the meridional wind on the bottom-right of Fig. 2 show bursts of amplitude that (apart from early 1990) match closely corresponding bursts in the band-passed zonal oscillations. Figure 3 plots the 20 day running averages of the time series at all heights in the range 70–100 km. These plots show that the intraseasonal oscillations evident in the smoothed time series of Fig. 2 are coherent in both amplitude and phase over a number of heights, further reinforcing the reality of these oscillations.

Thus clear intraseasonal oscillations of the winds at these heights are revealed by both spectral analysis and inspection of the velocity time series. That said, there are two occasions, in early 1993 and 1995, when the transitions to/from strong westward MLTSAO phases are so rapid that some spectral power will leak into higher harmonics of the zonal-velocity spectrum. Thus, some of the quasi-60 day enhancements in the band-passed zonal-velocity oscillations observed at these times may be contributed to by the MLTSAO. Enhancements observed at other times, however, and at all times in the meridional time series, are due to distinct quasi-60 day oscillations of the winds. Similarly, the peaks at ~40 days and 20–25 days in both time series cannot arise from a leakage of spectral power from the MLTSAO.

Figure 4 shows power spectra of the zonal and meridional velocity time series, plotted at their heights of observation. A corresponding power spectral density scale is given on the right: note that the meridional spectral scaling is an order of magnitude smaller than for the zonal spectra. We see that the peaks previously identified at 92 km in Fig. 2 occur over the height range 80–98 km. These spectra were also recomputed after applying Hanning, Parzen (triangular) and Welch (squared triangular) windows to the time series prior to Fourier transformation to minimize any spectral leakage. In all cases, the major peaks identified from Fig. 2 and evident in Fig. 4 occurred prominently.

Based on these spectra, we choose three principal pass bands (hereafter labeled A, B, and C) which are centered near the major peaks in the zonal velocity spectra. These bands are marked with rectangles in Fig. 4, indicating both the width and approximate height range of the signals we are trying to isolate. The Hanning filters we use to isolate fluctuations within each band are plotted with dotted curves above these shaded regions. The band-pass filters A and C are also applied to the meridional velocities, even though there are no distinct meridional peaks within band C. However, we replace filter B when analyzing

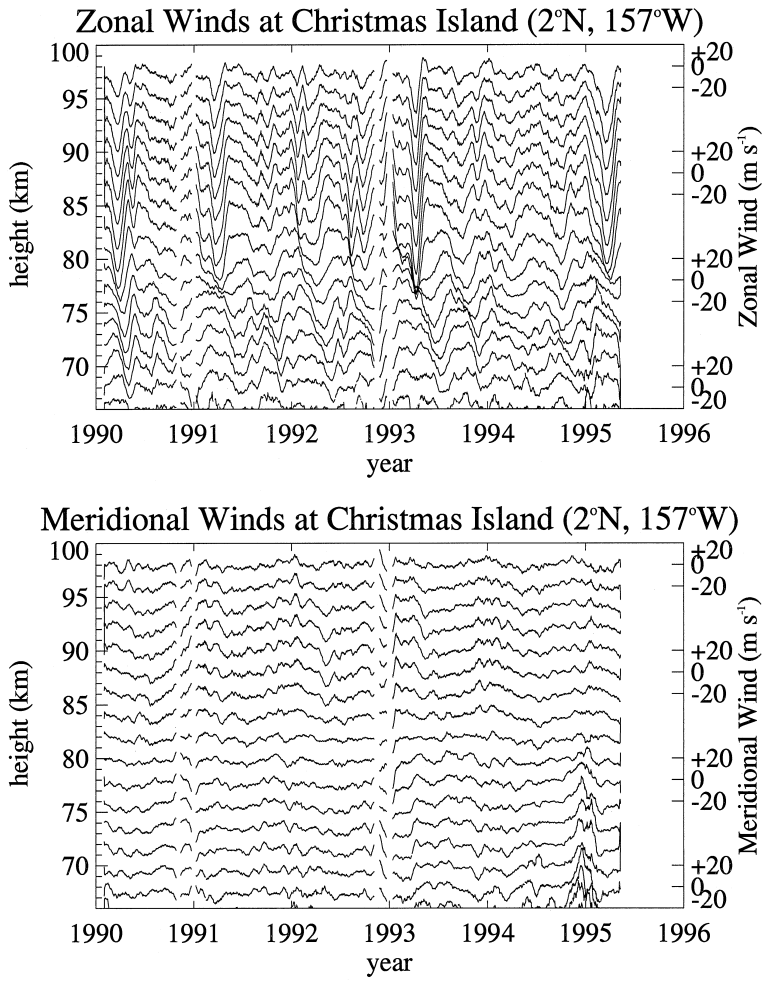

Fig. 3. Time–height plots of the time series of zonal and meridional winds after smoothing with a 20 day running average. The zero line of each time series is centered at the height of observation, with the top trace measured at 98 km. Corresponding velocity scales are shown on the right.

the meridional time series with a filter D which is displaced to slightly smaller periods, so that it is centered more on the peak at ~35 days in the meridional spectra in Fig. 4. Note that the filters A–C differ from those employed by Eckermann and Vincent (1994): filters A and B differ only slightly, whereas filter C isolates periods ~20–30 days in this study, whereas in Eckermann and Vincent (1994) it spanned periods ~15–25 days.

The periods or period ranges of some intraseasonal phenomena which could conceivably produce signals in our data are also shown in Fig. 4. Recent studies have shown evidence of the quasi-16 day Rossby normal mode in the mesosphere at middle to high latitudes (Williams and Avery, 1992; Forbes *et al.*, 1995) and in the equatorial ionosphere (Forbes and Leveroni, 1992; Parish *et al.*, 1995). Modeling by Forbes *et al.* (1995) suggests that the penetration of this disturbance into the equatorial mesosphere and thermosphere depends sensitively on background wind profiles and the effects of gravity-wave drag. There is no clear evidence of a 16 day signal in Fig. 4 (although there is a smattering of activity throughout the 12–20 day band within which this mode sometimes resides), nor is their much evidence of 16 day Rossby modes in the equatorial troposphere and stratosphere (Hirooka and Hirota, 1989). Clearly a quasi-16 day wave cannot account for the major peaks in Fig. 4. Similarly, lunar semidiurnal tides, while evident in mesospheric wind data from extratropical sites (e.g.,

Stening *et al.*, 1994), do not appear prominently in these data either: indeed, Stening *et al.* (1997) found amplitudes of no more than 1–2 m s^{-1} in these data. Neither is there much evidence for a response to the 27 day variation of incoming ultraviolet radiation due to solar rotation, which is known to influence mesospheric ozone and temperatures, particularly near the equator (e.g., Summers *et al.*, 1990; Hood *et al.*, 1991; Brasseur, 1993). Indeed, the only phenomena that appear to relate to the peaks we observe are the 30–60 day and 20–25 day oscillations of the equatorial troposphere (e.g., Hartmann *et al.*, 1992; Madden and Julian, 1994), as argued by Eckermann and Vincent (1994).

TIME–HEIGHT INTRASEASONAL VARIABILITY

Figure 5 profiles the zonal velocity activity within various period bands. The top plot shows the mean winds, obtained by retaining periods $\gtrsim 100$ days. The semiannual oscillation is clearly evident, showing, for example, that the first westward phase of the MLTSAO is usually stronger (e.g., Garcia *et al.*, 1997). Considerable interannual variability is also evident: for example, there are atypically strong first westward phases in early 1993 and 1995, whereas both westward phases are weaker and roughly equal during 1992 and 1997. Note also the much smaller semiannual oscillation below ~ 75 km. It is well-known that the amplitude of the semiannual oscillation is small, between about 60–70 km, effectively separating the stratospheric semiannual oscillation (SSAO) and the MLTSAO (e.g., Hirota, 1978; Garcia *et al.*, 1997). Band-passed fluctuations within bands A–C are displayed in the remaining three plots in Fig. 5, and again, the region below ~ 75 km is relatively quiescent, whereas at 80–98 km there are transient bursts of activity within all three bands.

Comparisons of Christmas Island MF radar winds with coincident wind measurements from UARS have suggested significant underestimations of the radar winds at lower heights, but much better agreement higher up (see Figs 11 and 12 of Burrage *et al.* (1996)). At these lower heights, the radar's data rates decrease, diurnal data coverage is incomplete, and clutter from ocean-wave echoes becomes a problem (Vincent and Lesicar, 1991), all of which could contribute to these apparent underestimations of wind speeds. Thus, the absence of intraseasonal peaks and the small MLTSAO below ~ 75 km may also be due in part to degraded instrument sensitivity at these lower heights.

The bursts of activity within bands A and B generally occur at similar times. As noted by Eckermann and Vincent (1994), the occurrence of activity in these bands is well correlated with the strength of the westward MLTSAO zonal winds. Since the first westward phase is usually stronger than the second, there tends to be more activity in bands A and B at the start of the year. Activity in band C, on the other hand, tends to appear in the middle to latter half of the year. Active regions within all three bands descend phase with time, in agreement with the initial study of bands A and B by Eckermann and Vincent (1994).

To study possible seasonal variations in the intraseasonal activity, we apply phase–time methods to the band-passed time series (e.g., Huang *et al.*, 1992). The basic method is depicted in Fig. 6. Its advantage here is that it provides time series of the peak amplitude $A(t)$ and phase $\phi(t)$ of the intraseasonal signals at the daily resolution of the original time series, unlike variance calculations which degrade the resolution to intraseasonal time scales (unless some sliding average is employed) and make seasonal trends harder to identify. Figure 7 displays seasonal variations of the peak amplitudes of the band-passed time series in Fig. 5. Despite the interannual variability evident within all three bands, we note weak but distinct annual variability in the mean seasonal curves. Band A shows greatest activity around December–April, and a similar tendency is weakly evident in band B. Conversely, band C shows greater activity on average during August–December.

Phase–time methods can also provide time series of frequency $\omega(t)$ (see Fig. 6), and hence the periods of various intraseasonal bursts of activity. Figure 8 profiles height variations of the period and peak amplitude of four bursts of band-A activity that occurred early in 1990, 1991, 1993, and 1995 (see Fig. 5). Activity typically peaks at ~ 86 km, but attenuates rapidly below 80 km as previously noted. Periods in these active regions are in the range 55–65 days, varying slightly from event to event, although the results also depend somewhat on the filter functions used. Similar calculations for four burst regions in band B (during early 1990, early 1992, late 1992, and early 1994) showed similar characteristics, with peak amplitudes ~ 5–8 m s^{-1} and periods ~ 40 days. Four burst regions in the band-C time series (in mid-1990, mid-1991, mid-1992, and late 1993) showed amplitudes peaking at ~ 5–8 m s^{-1} near ~ 85–90 km, attenuated amplitudes below 80 km, and periods typically ~ 22–24 days.

Figure 9 profiles the activity in the meridional velocities. The variations in the band-A activity are similar to those in Fig. 5, and these active regions also exhibit phase descent with time. The peak of the activity tends to occur typically ~ 90 km, slightly

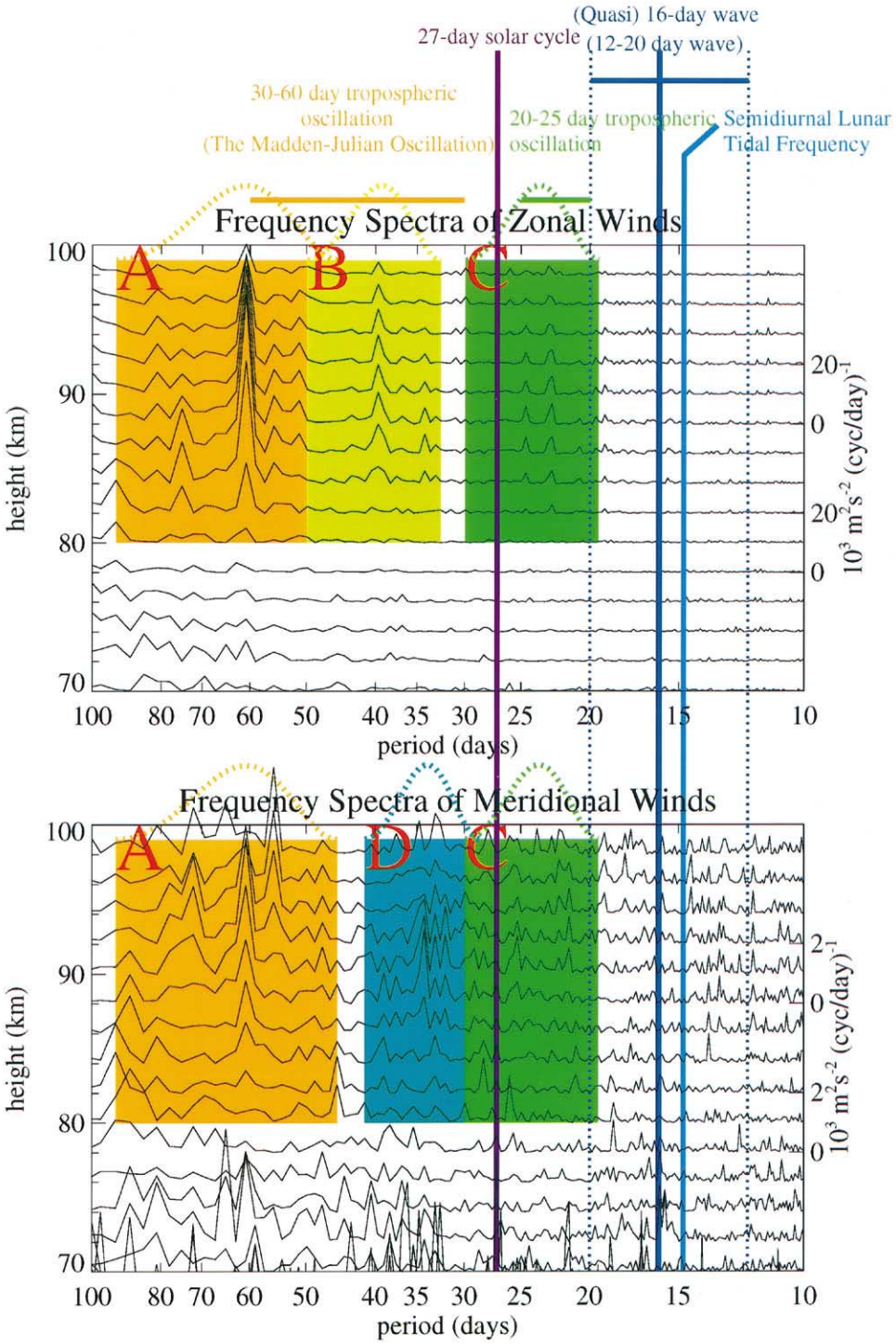

Fig. 4. Power spectral densities of zonal and meridional velocities within the intraseasonal band, with the zero line plotted at the height of observation. Spectral units are given on the right. Bands A–C are marked on these plots, and the Hanning filters used to isolate these peaks are plotted with dotted curves above the marked areas. Periods and period ranges of other intraseasonal geophysical phenomena are depicted on the plot.

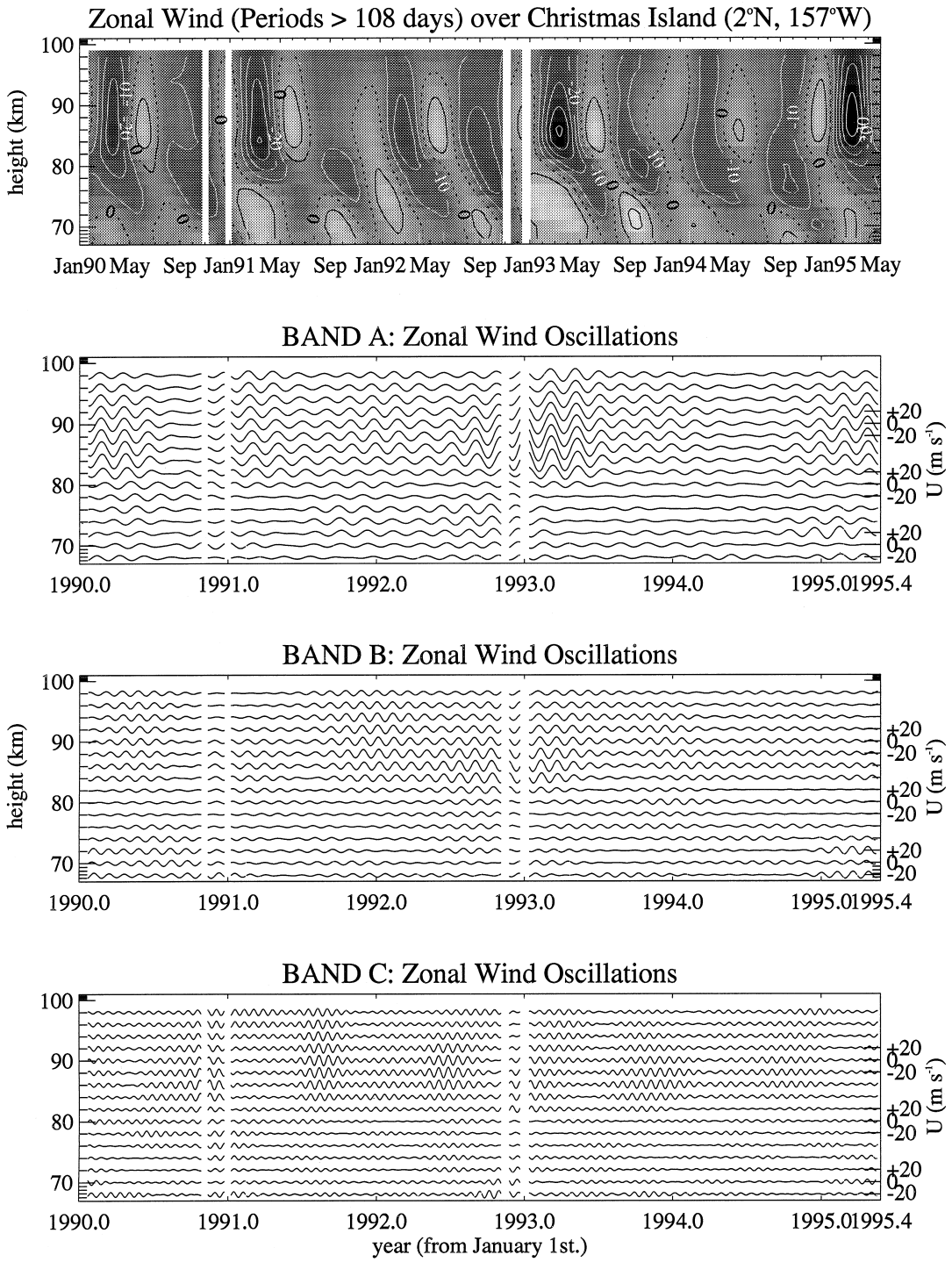

Fig. 5. Time–height plots of the band-passed time series of zonal winds at various heights are shown in the bottom three plots for filters A–C. An amplitude scale for these time series is shown on the right. The activity in these oscillations can be compared with activity in the top plot, which shows contours of zonal winds in which periods $\gtrsim 100$ days have been retained, which we take to represent mean-flow variations. Contour labels are in $m\,s^{-1}$, and westward (eastward) values are negative (positive) and have darker (lighter) shading and solid white (black) contours. The contour interval is $10\,m\,s^{-1}$. Zero wind lines are dotted.

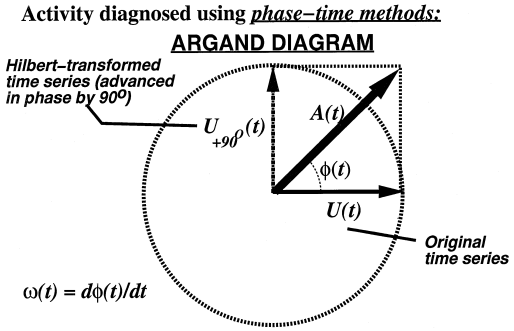

Fig. 6. Diagram showing the basis of the phase–time method. The original time series $U(t)$ is combined with its Hilbert transform, which we approximate here by applying 90° phase shifts to each harmonic of the Fourier transform of $U(t)$, then retransforming to yield $U_{+90^\circ}(t)$. The two time series are combined into a complex vector time series (solid vector) which provides both the peak amplitude $A(t)$ (the length of the solid vector) and the phase $\phi(t)$. A time series of frequency follows from $\omega(t) = d\phi(t)/dt$.

higher than for the zonal activity. The major difference, however, is that the meridional oscillations in band A are out of phase with the zonal band-A oscillations. This is shown in Fig. 10a, which plots time hodographs of the total (zonal and meridional) band-A velocities at 90 km. An anticorrelation between the band-A velocity components is apparent, with correlation coefficients of around −0.75 at this height over the full 1944 days of data (Fig. 10b).

CORRELATIONS WITH GRAVITY WAVE AND TIDAL ACTIVITY

Figure 11 plots time series of the zonal and meridional winds from Fig. 3, along with the peak zonal amplitude of the diurnal tide, and zonal and meridional velocity variances in the 12 min–4 h band, the latter indicative of gravity-wave activity. At times when intraseasonal activity was strong (e.g., early in 1990, 1991, and 1993), we see intraseasonal oscillations of zonal gravity-wave variances and diurnal tidal amplitudes above ~80–85 km which are coherent in phase with height. The meridional velocity variances tend to show strongest intraseasonal oscillations above about 90 km.

To investigate the gravity-wave variability further, we compute power spectra of the unsmoothed time series of zonal and meridional velocity variances, to delineate any periodicities in the wave activity (e.g., Isler and Fritts, 1996; Connor and Avery, 1996). The spectra at 86–90 km are shown in Fig. 12a. A strong peak at ~60 days is evident at 86–90 km in the zonal variances, which clearly is very similar to the quasi-60 day band-A peak in the zonal wind spectra from Fig. 4. The intraseasonal variations at 86–90 km are greater for the zonal variance than for the meridional variance. There are suggestions of additional periodicities in both velocity variances at ~40 days (band B), and ~25 days (band C), although these peaks are quite weak and may not be significant.

The variance spectra above 86–90 km change markedly. In Fig. 12b we note that intraseasonal variations in zonal variance at 92–98 km are of similar magnitude to those at 86–90 km. The peak at 60 days, however, has been strongly dissipated (along with the weak 40 day and 25 day peaks), consistent with a transfer of these periodicities in gravity-wave activity into the mean flow through the 86–98 km height range, as hypothesized by Eckermann and Vincent (1994). The zonal variance spectrum at 92–98 km now peaks nearer 45 days. Intraseasonal variations of meridional activity at 92–98 km are large and exceed the zonal variations. A strong peak in the meridional variances now occurs at ~60 days, with subsidiary peaks at ~90 days and ~45 days.

Figure 13 shows spectra of time series of the peak zonal and meridional amplitudes of the diurnal tide. Again, a quasi-60 day peak is evident. However, the zonal tidal amplitudes also show large distinct peaks centered at ~40 days and ~24 days, which are very similar to the peaks within bands B and C of the zonal-wind spectra in Fig. 4 and far exceed the weak peaks in the gravity-wave variances in Fig. 12a.

The intraseasonal tidal activity and the attenuation (intensification) of intraseasonal variations of zonal (meridional) gravity-wave activity with height are all well illustrated during the strong MLTSAO phase in early 1993. The winds, zonal tidal amplitudes, and gravity-wave activity for the first six months of 1993 are replotted in Fig. 14. We see strong intraseasonal variations in zonal gravity-wave variance which attenuate with height, consistent with the perceived role of this gravity-wave activity in driving both the strong westward MLTSAO winds and intraseasonal wind variability. We also note a very strong diurnal tide with an intraseasonal activity variation which attenuates with height, which may also drive these strong westward winds. The strong colocated gravity-wave and tidal activities also produce strong gravity-wave tidal interactions in these data (see also Nakamura *et al.*, 1997). The intensification of meridional variance at upper heights is also very apparent, as is its intraseasonal variation. We tentatively associate this with the filtering of more meridionally directed waves by the intraseasonal flow variations that appear at ~80–90 km. Note the quasi-bimonthly variations in all five plots.

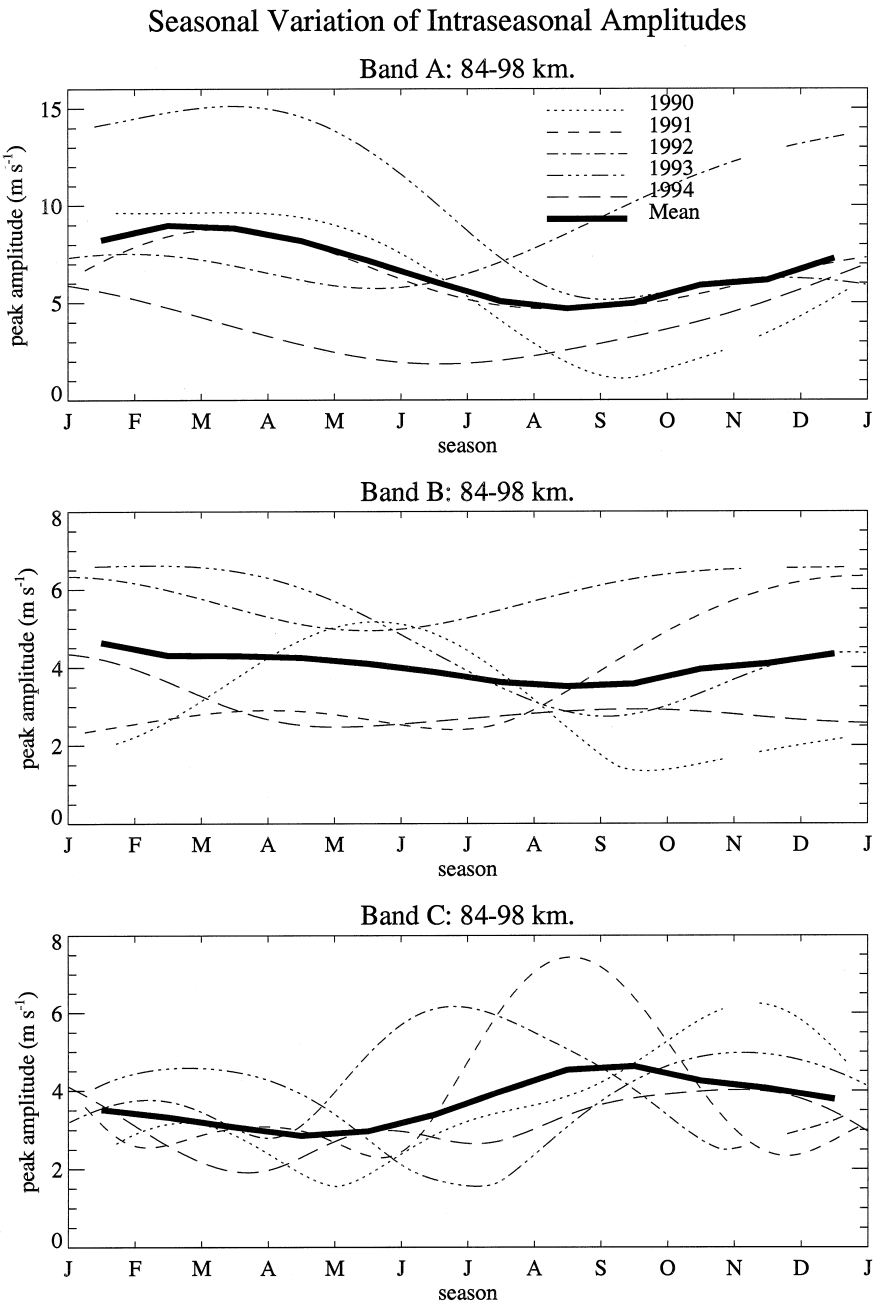

Fig. 7. Seasonal variations of peak amplitudes of the band-passed zonal wind time series profiled in Fig. 5. Various broken curves show the trends for individual years, while the thick curve shows the mean seasonal variation from 1990–1994.

DISCUSSION

We have identified three distinct bands of intraseasonal activity in these MLT wind data, centered at ~60 days (band A), 35–40 days (bands B and D), and 20–25 days (band C). Similar periodicities have also been detected in diurnal tidal amplitudes and gravity-wave variances at these heights. We have also pre-

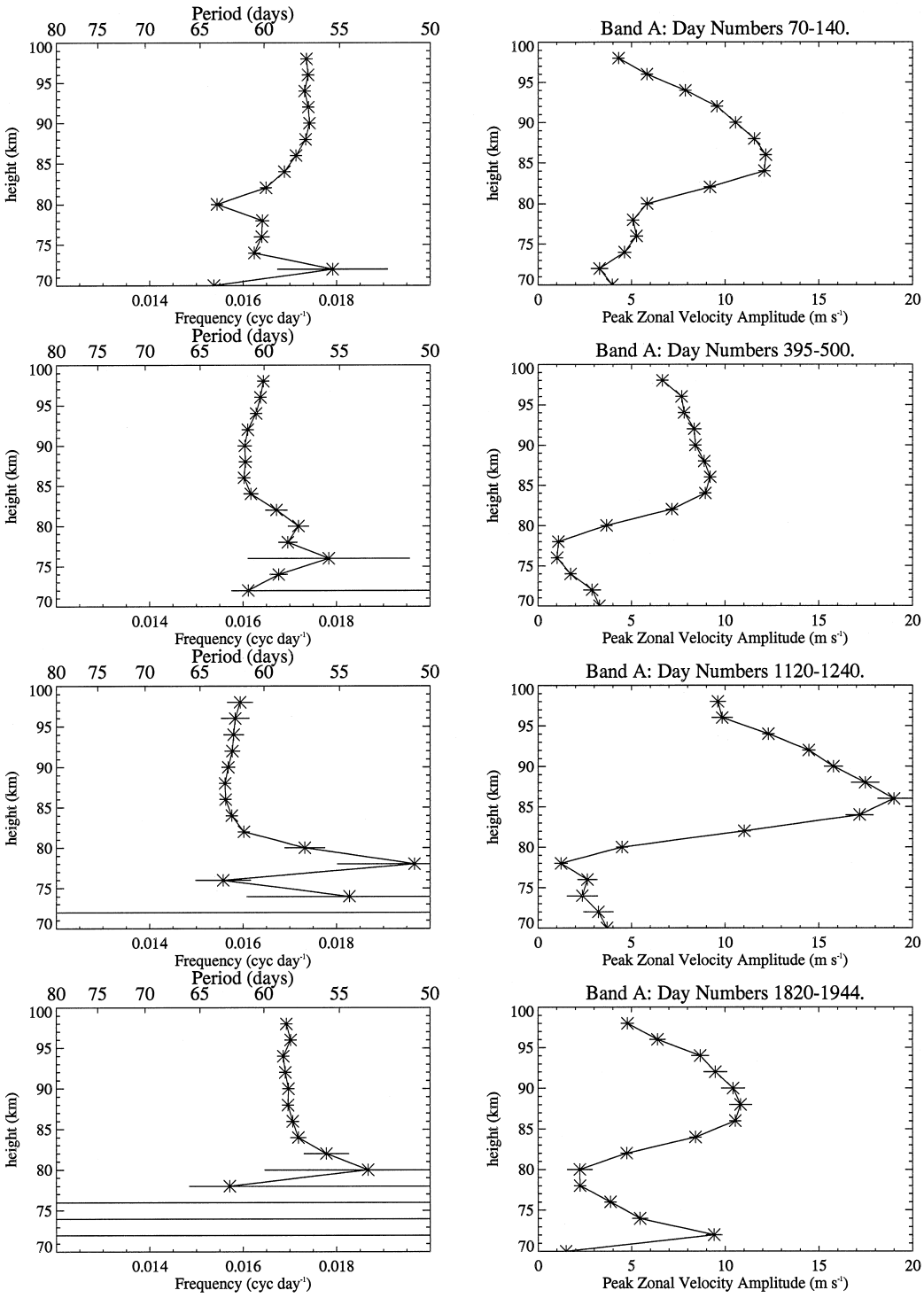

Fig. 8. Altitude profiles of period (left column) and peak zonal velocity amplitude (right column) for four separate bursts of activity within band A. The day number ranges are shown on the plot, where day 1 is January 1, 1990. Error bars are standard errors of the mean derived from the time series of amplitude and phase provided by phase–time methods.

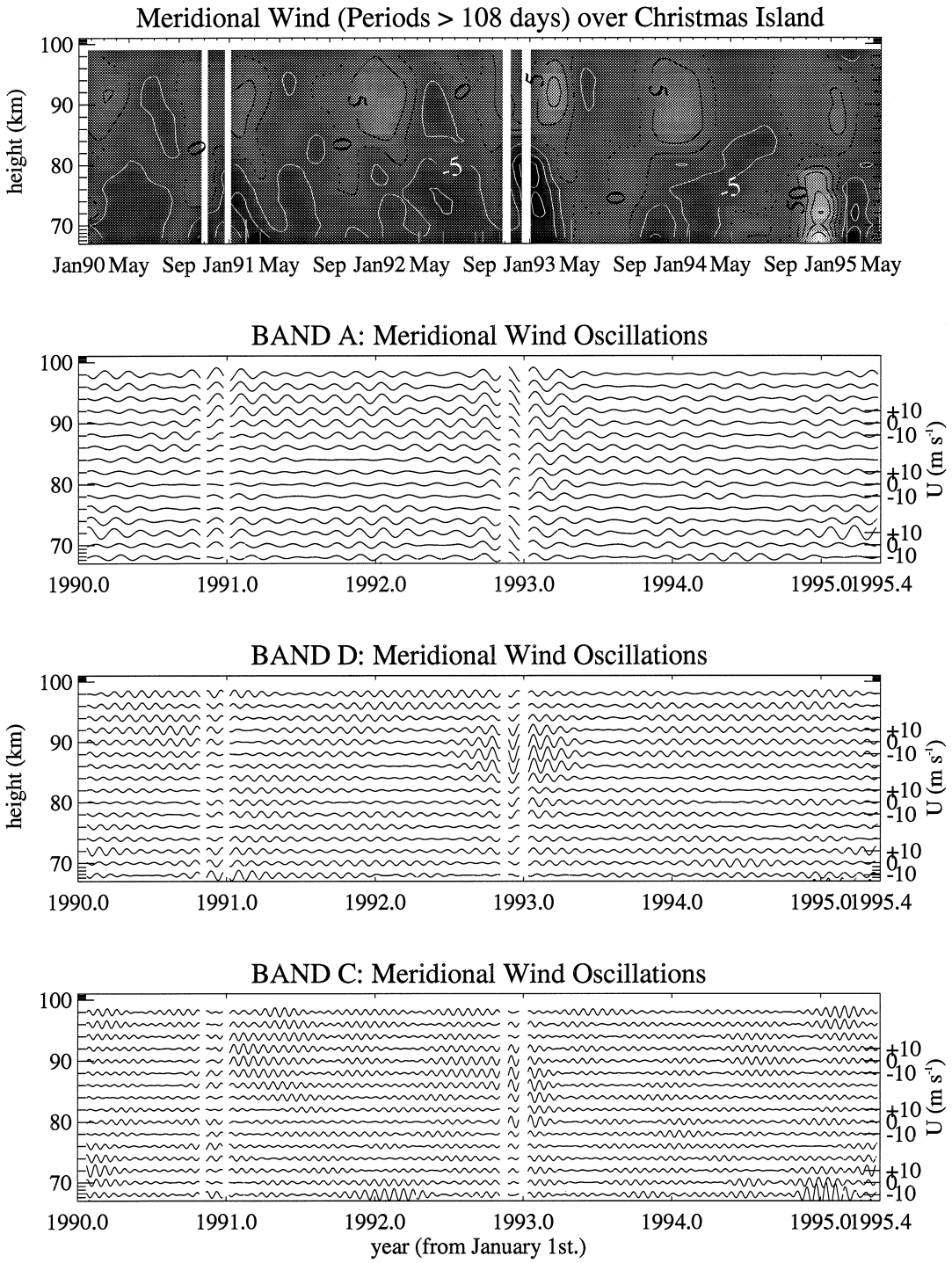

Fig. 9. Analogous presentation to Fig. 5, but this time for meridional winds. The amplitude scale for the band-passed fluctuations is shown on the right of the bottom three plots. The contour interval in the top plot is 5 m s^{-1}, and southward values are negative and have darker shading and white solid contours. Note that filter B is replaced by filter D in this case.

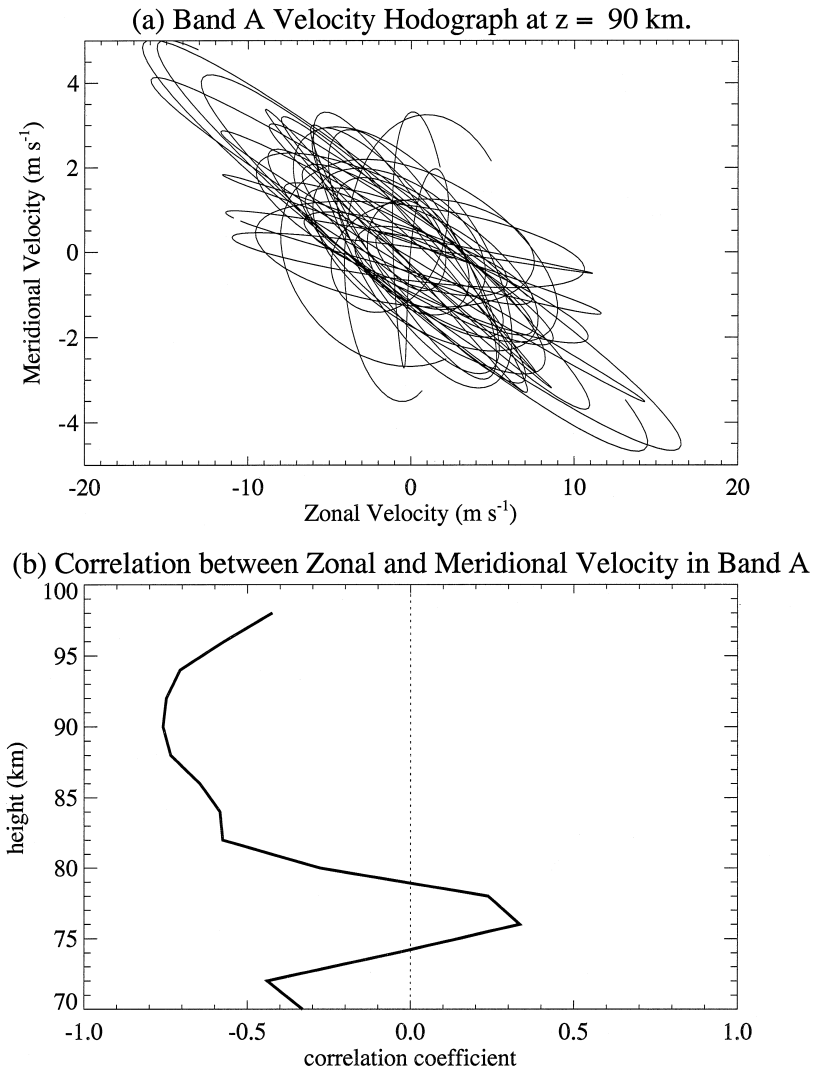

Fig. 10. (a) Hodograph of the band-A velocity oscillations at 90 km. (b) Height variation of the correlation coefficient between the zonal and meridional velocity time series within band A.

sented preliminary evidence (summarized in Fig. 4) that these intraseasonal winds may be associated with the 30–60 day and 20–25 day oscillations encountered in the equatorial troposphere, as postulated by Eckermann and Vincent (1994).

We investigate this in more depth here. Since the data from Christmas Island comprise our only explicit information on intraseasonal oscillations of the equatorial MLT region to date, firm conclusions on the nature and origin of this activity are difficult to draw. Our discussion is developed with this limitation in mind, and is structured as follows. First we briefly describe the salient characteristics of observed tropical tropospheric intraseasonal variability (TTIV). Next, based on some recent observations in and around India, we briefly reconsider whether planetary waves associated with TTIV could propagate directly to mesospheric heights. Finally, on the weight of current evidence, we propose an explanation for the intraseasonal oscillations we observe based on gravity-wave and diurnal-tidal driving of the MLT flow, and go on to investigate some possible consequences.

Tropical tropospheric intraseasonal variability (TTIV)

The 30–60 day tropospheric oscillation is an intensively studied phenomenon, and is known as the Mad-

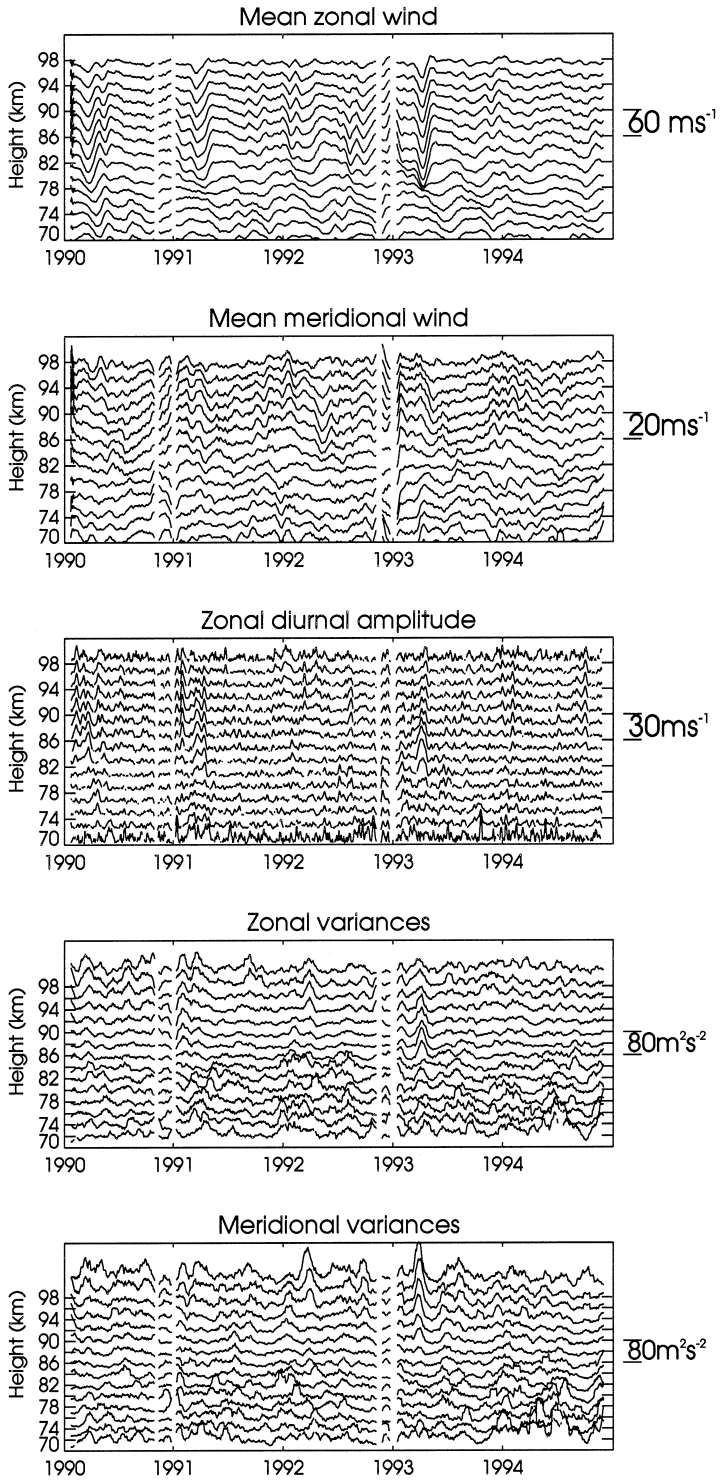

Fig. 11. The top two plots reproduce time series from 1990–1994 of zonal and meridional winds from Fig. 3. The middle plot shows peak zonal amplitudes of the diurnal tide. The bottom two plots show gravity-wave variances in zonal and meridional velocities within the 12 min–4 h period range. The gravity-wave time series were smoothed with a 10 day running average, and the tidal data with a 6 day running average.

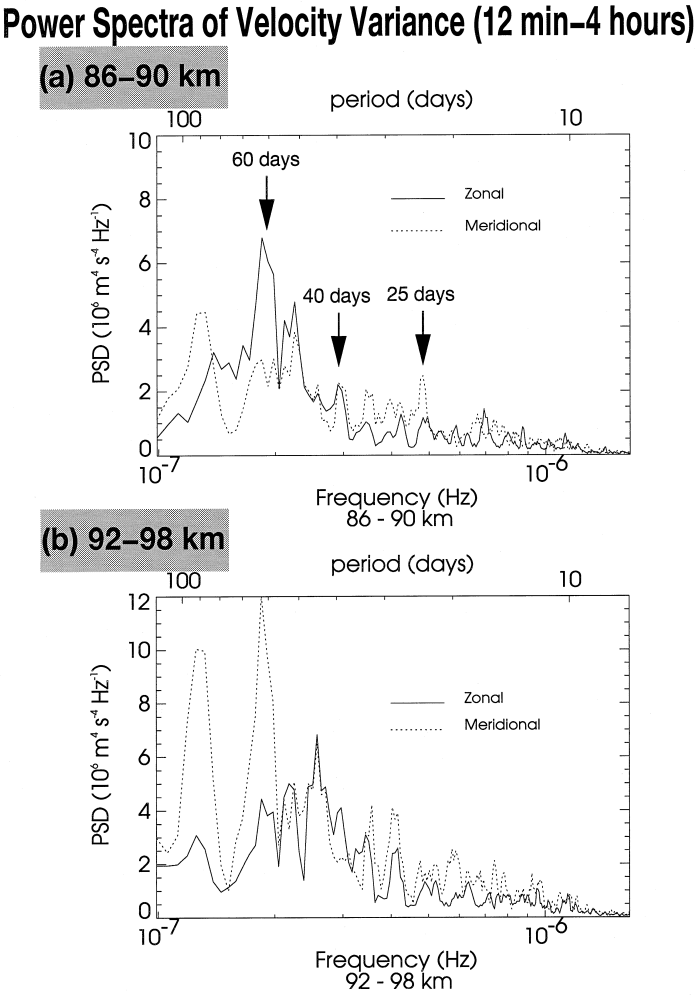

Fig. 12. Power spectra of time series of zonal and meridional velocity variance in the 12 min–4 h band: (a) 86–90 km; (b) 92–98 km. These spectra were smoothed with a 3-point running average.

den–Julian oscillation (MJO), after its discoverers (see the review of Madden and Julian (1994)). It occurs when a large region of convective ascent moves eastward from the Indian Ocean into the western Pacific (Madden and Julian, 1972), producing 30–60 day periodicities in regional convective activity as it passes (see, e.g., Hartmann and Gross 1988; Salby and Hendon, 1994; Dunkerton and Crum, 1995). This disturbs the climatological Walker circulation, producing a planetary-scale response of similar period in the equatorial velocity field. This velocity response can be understood to first order as a coupled Kelvin–Rossby mode near the forcing region, which, as one shifts further eastward, is replaced by a wavenumber-1 Kelvin wave radiating away from this forcing zone (e.g., Parker, 1973; Hendon and Salby, 1994, 1996; Salby *et al.*, 1994).

A strong 20–25 day tropical oscillation has also been detected over the western Pacific (Ghil and Mo, 1991; Hartmann *et al.*, 1992; Kiladis *et al.*, 1994) and elsewhere (e.g., Anyamba and Weare, 1995). While this particular oscillation seems to be distinct from the MJO, it should also be noted that the MJO's period range can vary considerably, and occasionally approaches 25 days (e.g., Hayashi and Golder, 1993; Madden and Julian, 1994).

Can TTIV propagate into the middle atmosphere?

Eckermann and Vincent (1994) argued on theoretical grounds that the mesospheric intraseasonal

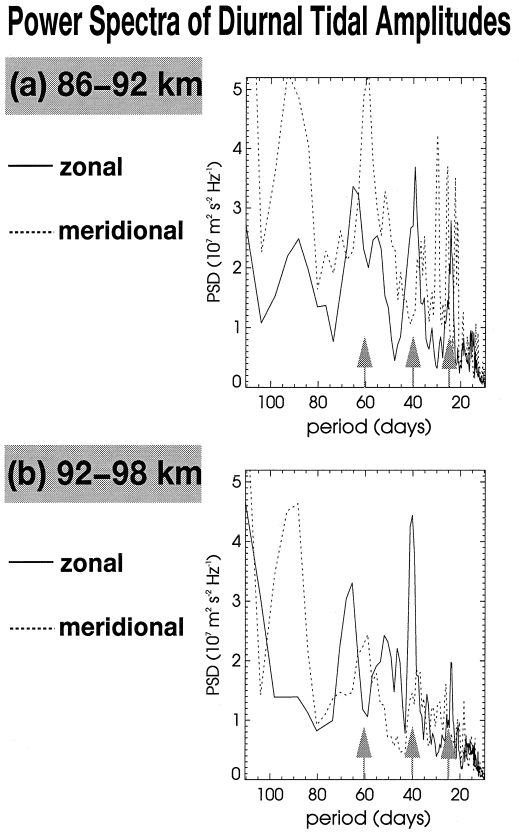

Fig. 13. Power spectra of time series of the peak zonal (solid curve) and meridional (dotted curve) velocity amplitudes of the diurnal tide: (a) 86–92 km; (b) 92–98 km. These spectra were smoothed with a 3-point running average.

activity observed at Christmas Island was unlikely to result from direct upward propagation of the planetary waves associated with the MJO. However, some recent observations in the Indian sector lead us to reconsider this possibility here.

It is well known that MJO activity attenuates rapidly above the tropopause (Madden and Julian, 1971), and studies of rocket and radiosonde data from tropical Indian stations show this quite clearly (Nagpal and Raghavarao, 1991; Nagpal *et al.*, 1994; Kumar and Jain, 1994). However, Nagpal and Raghavarao (1991) showed that intraseasonal power in their rocket wind data reintensified somewhat in the upper stratosphere. This was investigated further by Nagpal *et al.* (1994) and Kumar and Jain (1994) using rocket data from three Indian stations spanning 8.5°–21.5°N (shown in Fig. 1). They noted increased intraseasonal activity in both zonal and meridional winds at ~50 km, most notably at the two higher-latitude sites. Since there were nearly equal amounts of intraseasonal activity in both wind components, they concluded that this was inconsistent with Kelvin waves, and associated the activity with Rossby waves. Nagpal and Raghavarao (1991) argued that these Rossby waves propagated into the tropical upper stratosphere from mid-latitudes (see also Nagpal *et al.* (1994)), whereas Kumar and Jain (1994) suggested that the waves 'leaked' into the upper stratosphere from the tropical troposphere via vertical propagation. The latter is possible since the MJO contains a significant Rossby-wave component, particularly in forcing zones near India (e.g., Hendon and Salby, 1994).

Ziemke and Stanford (1991) studied Rossby waves of intraseasonal period (1–2 months) in eight years of daily global geopotential height data from British Meteorological Office analyses. They focused on strong wave activity in a longitude zone near the east coast of India. This activity, initially concentrated in the equatorial troposphere, propagated into the extratropical upper troposphere and stratosphere to form a regional dipole pattern about the equator. Similar patterns are also observed at periods ~25 days (Anyamba and Weare, 1995). Thereafter, the waves continued propagating upwards, refracting back into the tropical stratopause region (see Figs 5 and 6 of Ziemke and Stanford (1991)). Similar Rossby-wave propagation paths are suggested in the model simulations of Salby *et al.* (1994) (e.g., their Fig. 18). This sort of wave propagation path could clearly explain the reemergence of intraseasonal activity observed in the Indian rocket data near the stratopause: if so, then the explanations of it offered by Nagpal and Raghavarao (1991) and Kumar and Jain (1994) are essentially both correct.

These rocket and satellite data, however, cut out at ~60 km, and so it is unclear whether these waves reach the mesosphere and lower thermosphere. GCM simulations by Hayashi and Golder (1993) show penetration of equatorial Rossby-wave activity at intraseasonal periods to near the top of their model (~75 km), which is still below the region of activity observed in our data (~80–98 km). However, the presence of Rossby waves at the tropical stratopause is only feasible during the eastward phases of the SSAO. Since the antiphased MLTSAO will be westward at these times, equatorial Rossby waves will be absorbed at critical levels somewhere between the SSAO and MLTSAO. Thus direct Rossby-wave propagation into the ~80–98 km region of the equatorial atmosphere seems unlikely at these times. However, any intraseasonal Rossby-wave oscillations at the stratopause could affect the transmissivity of gravity waves through the tropical stratopause, thereby forcing a mesospheric disturbance of similar period

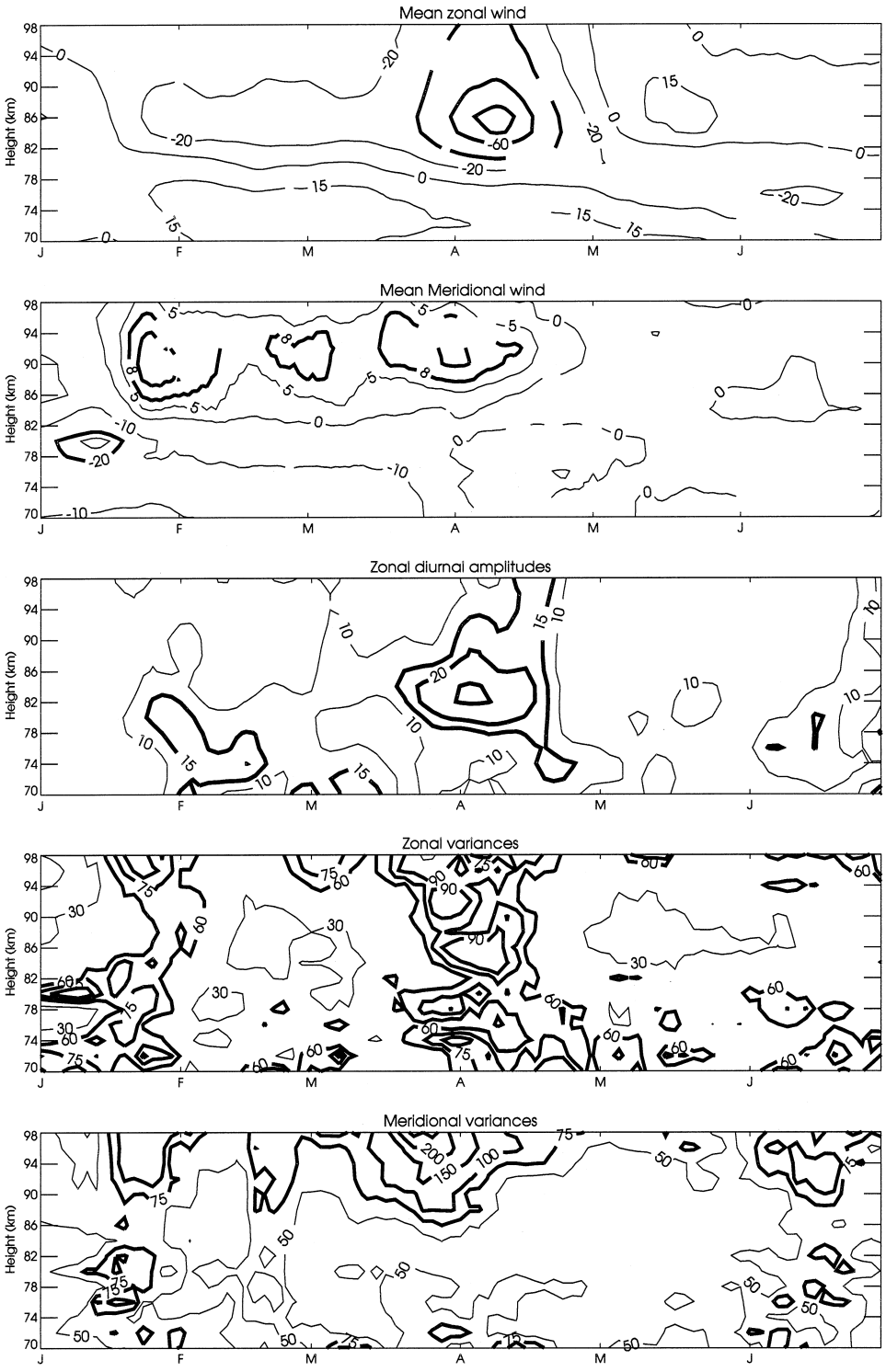

Fig. 14. As for Fig. 11, but focusing on the first six months of 1993, with the data plotted in contour form. Contour labels are in $m\,s^{-1}$ for the mean winds and zonal diurnal tidal amplitudes, and in $m^2\,s^{-2}$ for the velocity variances. Active regions in the data are highlighted with heavier contours.

through modulated gravity-wave breaking. Very similar processes have been proposed in the mid-latitude Northern Hemisphere during winter (Holton, 1984; McLandress and McFarlane, 1993; Smith, 1996).

Intraseasonal activity in the mid-Pacific MLT region

Our mid-Pacific observations at MLT heights have shown that intraseasonal activity within bands A and B occurs preferentially during westward phases of the MLTSAO. As mentioned, any equatorial Rossby waves have probably been removed at critical levels lower down, but since the SSAO is eastward at these times, intraseasonal Rossby waves could be present at the stratopause to modulate gravity-wave transmissivity and force a related mesospheric disturbance (Holton, 1984). Kiladis and Wheeler (1995) have observed Rossby waves with periods $\sim$6–30 days in the troposphere near Christmas Island, although whether these waves could propagate into the tropical upper stratosphere is unclear. GCM simulations by Hayashi and Golder (1993) produced significant intraseasonal Rossby-wave activity throughout the equatorial stratopause.

However, there are several reasons for supposing that much of the activity at 80–98 km over Christmas Island is not produced either directly or indirectly by middle-atmosphere Rossby waves. First, Rossby-wave oscillations or Rossby-wave-modulated gravity-wave breaking might be expected to accelerate zonal and meridional winds fairly equally (see e.g., Kumar and Jain, 1994), whereas the bulk of the intraseasonal activity we observe here is zonal. The activity over Christmas Island is more suggestive of either a zonal-wind vacillation or of a Kelvin wave (Eckermann and Vincent, 1994). Indeed, the data of Ziemke and Stanford (1991) suggest that the upper-stratospheric Rossby waves they studied were confined to a fairly narrow longitude zone near India, and so may be less relevant to our observations in the central Pacific.

This perceived longitudinal difference in the character of intraseasonal activity at the Indian stratopause and in the mid-Pacific MLT region has interesting similarities with the MJO. In the forcing region in and around Indonesia and India, MJO activity is characterized by a combined Kelvin–Rossby wave response, whereas at longitudes well away from the forcing region the activity is dominated by a pure (zonal) Kelvin wave response (Hendon and Salby, 1994, 1996). Tropospheric radiosonde data from Kanton (formerly Canton Island), which is very near Christmas Island (see Fig. 1), bear this out. They reveal a strong peak in the zonal wind at $\sim$40–50 days (Madden and Julian, 1971; Hartmann and Gross, 1988) produced by a large-amplitude Kelvin wave which has propagated eastward to Kanton from its forcing region to the west (Hendon and Salby, 1994).

The MJO-related Kelvin waves over Kanton attenuate rapidly above $\sim$80 hP (Madden and Julian, 1971), supporting theoretical assessments that they cannot propagate vertically to MLT heights (Eckermann and Vincent, 1994). Since they are equatorially ducted, an extratropical propagation path into the upper atmosphere, like the one chronicled for Rossby waves by Ziemke and Stanford (1991), is also infeasible. How, then, might similar signals reach the mid-Pacific mesosphere?

Gravity waves, tides, and TTIV-influenced convective activity

Eckermann and Vincent (1994) suggested that MJO-modulated convection could produce an intraseasonal variation in the intensity of convectively generated gravity waves entering the middle atmosphere. Models have shown how the dissipation of convectively generated waves can greatly influence the circulation of the middle atmosphere (e.g., Pfister *et al.*, 1993a; Alexander, 1996). Selected aircraft missions during the Panama 80 and STEP 87 campaigns (in regions shown in Fig. 1) revealed strong stratospheric gravity-wave activity emanating from tropical tropospheric convective systems (Pfister *et al.*, 1993a, b; Alexander and Pfister, 1995).

Here we have noted correlations between intraseasonal variations in MLT winds and similar periodicities in gravity-wave activities at 80–98 km. The relations at 86–90 km are superficially consistent with a 60 day MJO-controlled variation in the intensity of convectively generated gravity waves produced in the troposphere (Fig. 12). However, similar cycles in wave variance could conceivably have resulted from gravity waves interacting with a preexisting quasi-60 day wind oscillation at these heights (e.g., Vincent and Eckermann, 1990; Isler and Fritts, 1996).

Some evidence for the hypothesized MJO modulation of gravity-wave generation by convection in the tropical Pacific was provided recently by Karoly *et al.* (1996). They analyzed several months of high-resolution radiosonde data from Santa Cruz (see Fig. 1) in the tropical south Pacific. It is well-known that convective activity in and around this region is influenced by the MJO (see e.g., Hartmann and Gross, 1988) as eastward-moving intraseasonal convective zones drift southward towards the South Pacific Convergence Zone (e.g., Kiladis and Wheeler, 1995). The observations of Karoly *et al.* (1996) were taken during

the 4 month TOGA COARE observational campaign, starting in November, 1992 when the MJO was active and dominated regional convective activity (Gutzler *et al.*, 1994; Sheu and Liu, 1995). They noted statistically significant correlations between stratospheric gravity-wave activity in their data and outgoing longwave radiation in the region, the latter a standard proxy for convective activity. Thus, during this period, there appear to be clear MJO-related influences on the intensity of gravity waves entering the middle atmosphere.

We have seen even clearer intraseasonal periodicities in the amplitude of the diurnal tide (Fig. 13). Convective activity in the equatorial troposphere has a strong diurnal variation (e.g., Hendon and Woodberry, 1993) which, through latent heat release, can provide an important thermal forcing of tidal structures (Hamilton, 1981). Modeling has shown that diurnally varying convective activity forces a rich spectrum of nonmigrating diurnal tidal modes in the atmosphere (Lieberman and Leovy, 1995; Williams and Avery, 1996), and the largest-scale modes can propagate into the equatorial MLT region with significant amplitudes (Lieberman, 1991; Lieberman and Leovy, 1995). Given the intraseasonal variations in equatorial convective activity that also occur (e.g., Hartmann and Gross, 1988), then it seems likely that combined diurnal and intraseasonal variations in convection will yield intraseasonal variations in the amplitude of convectively forced diurnal tides in the MLT region, as we observed in Fig. 13.

Eckermann and Vincent (1994) argued that MJO-modulated gravity-wave activity might propagate into the mesosphere and dissipate, forcing similar MJO-related periodicities in mesospheric winds. The same argument also holds for diurnal tides, which dissipate at equatorial MLT heights and can provide substantial mean-flow forcing (e.g., Hamilton, 1995). Indeed, comparison of Figs 12 and 13 suggests that diurnal tides may be more important than gravity waves in forcing the intraseasonal zonal-wind activity within bands B and C (Fig. 4). The intraseasonal variations we have observed in gravity-wave activity, tidal activity, and winds in these MLT data, coupled with the lower-atmosphere observations of Karoly *et al.* (1996), provide some preliminary observational support for gravity/tidal-wave forcing of intraseasonal MLT winds near the equator. We now develop these ideas in a little more theoretical depth, and then apply them to investigate how TTIV-controlled gravity-wave and tidal activity could produce some of the observed intraseasonal periodicities we see in the MLT winds.

Intraseasonal gravity-wave and tidal forcing of winds in the equatorial MLT region

Near the equator, the zonally averaged momentum budget can be described quite accurately by the simplified equation (e.g., Bacmeister *et al.*, 1995)

$$\frac{D\bar{U}}{Dt} = X_{mech}, \tag{1}$$

where $D/Dt = \partial/\partial t + v^*\partial/\partial y + w^*\partial/\partial z$, ($v^*$, w^*) are the velocities of the residual meridional circulation, $\bar{U}$ is zonal velocity and X_{mech} is a mechanical forcing term which, at MLT heights, is dominated by gravity waves and tides. Clearly from equation (1), the Lagrangian evolution of the equatorial zonal flow is strongly controlled by X_{mech} variations due to wave forcing, as models of the quasi-biennial oscillation, SSAO, and MLTSAO have demonstrated.

However, coherent time variations in wave activity may also influence $\bar{U}$. The influence that diurnal variations in convectively generated gravity waves could have on tidal structures was investigated by Eckermann and Marks (1996). They showed that a time variation in wave-field intensity yielded a time-varying X_{mech} contribution, whereupon equation (1) can be reexpressed as

$$\frac{D\bar{U}}{Dt} = \frac{1}{\rho}\frac{\partial P_x}{\partial t} + X_{diss}, \tag{2}$$

where X_{diss} is a forcing due to wave dissipation and turbulent diffusion, ρ is background density and P_x is the total pseudomomentum density of the wave field. Equation (2) clearly shows that, even when small-scale dissipation is limited ($X_{diss} \approx 0$), strong Lagrangian accelerations of the zonal flow can result from local time variations in the total wave pseudomomentum density impinging upon the mesosphere.

Here we associated P_x with the total pseudomomentum density due to gravity waves and diurnal tides in the equatorial MLT region. Our analysis showed strong intraseasonal variations in wave variances and tidal amplitudes (see Figs 12 and 13). Given realistic assumptions about wave field anisotropy and energy distributions, similar periodicities in P_x may also be expected (e.g., Fritts and VanZandt, 1993), whereupon $\partial P_x/\partial t$ will have large peaks at periods $\sim$60 days, $\sim$40 days, and $\sim$25 days. From equation (2), we see that for the simplified situation of $X_{diss} = 0$ and $D/Dt \approx \partial/\partial t$, then zonal wind accelerations follow $\rho^{-1}\partial P_x/\partial t$. Thus intraseasonsal peaks in $\partial P_x/\partial t$ (e.g., Fig. 13) can appear in $\partial\bar{U}/\partial t$ and hence in $\bar{U}$, as observed in Fig. 4.

Of course $X_{diss} \neq 0$ and $D/Dt \neq \partial/\partial t$ at MLT heights,

so that while transience may play an important role, X_{diss} is also large at these heights and will play a primary role in the mean-flow evolution. Dissipation of intraseasonally modulated wave and tidal activity at MLT heights is also likely to produce intraseasonal periodicities in X_{diss}, leading via equation (2) to a more complicated mean-flow evolution (see e.g., Section 4.10 of Baines (1995)) which should also result in an intraseasonal variation in $\bar{U}$, as argued by Eckermann and Vincent (1994). Additional influences, such as nonzonal wave breaking and meridional transport $\left(\frac{D}{Dt} \neq \frac{\partial}{\partial t}\right)$, may also induce similar periodicities in v^* to those observed in Fig. 4.

While we have presented both observational and theoretical evidence to support gravity-wave and tidal driving of intraseasonal oscillations in the middle atmosphere, more detailed numerical modeling will be needed to assess this mechanism fully. Interestingly, Held *et al.* (1993) documented a 60 day stratospheric oscillation that arose naturally within a tropical numerical model which contained realistic parameterizations of radiation, moisture and convection. This oscillation was presumed to be forced by convectively generated gravity-wave activity in the model. While these model results and our observations differ in many ways (different heights, no semiannual oscillation in their model, and so on), their study at least establishes a precedent for the forcing of intraseasonal wind oscillations in the tropical middle atmosphere by convectively generated waves.

Our theoretical discussion has assumed, for simplicity, that the peaks in Fig. 4 are caused by mean wind variations over intraseasonal time scales. Ground-based data such as these, however, cannot tell us whether they are indeed mean-flow vacillations (wavenumber 0) or are instead due to planetary-wave disturbances (wavenumbers ≥ 1). In fact, either is possible, as discussed by Eckermann and Vincent (1994). Since MJO-modulated convection occurs within narrow longitude zones rather than uniformly around the equator (e.g., Dunkerton and Crum, 1995), this will yield a zonally asymmetric distribution of gravity waves emanating from convective zones. Simulations by Williams and Avery (1996) also reveal longitudinal variations in convectively forced tidal activity in the equatorial MLT region. This zonally asymmetric wave activity could force an intraseasonal planetary wave in the MLT region (e.g., Holton, 1984). However, similar longitudinally confined convection existed in the model of Held *et al.* (1993) yet the ensuing 60 day stratospheric oscillation appeared in the mean zonal wind. Since equatorial convection generates waves with a range of zonal wavenumbers (e.g., Bergman and Salby, 1994), then the mean-flow driving produced by such a broad spectrum of waves may not favor the generation of pure planetary-wave modes at MLT heights. The oblique zonal propagation of equatorial modes and gravity waves away from convective zones may also lead to a more symmetric zonal distribution of wave activity at heights some distance above the convection (e.g., Alexander, 1996) and thus to a more zonally symmetric flow forcing. Since there are also strong gravity wave-tidal interactions in our data (see also Isler and Fritts, 1996; Connor and Avery (1996)), this will lead to mutual interactions among the mean flow, the intraseasonal flow, tidal oscillations and gravity waves, the net results of which are difficult to predict at present. Satellite observations should help to clarify the true zonal structure of the intraseasonal MLT winds.

Origin of intraseasonal periodicities in the MLT region

One difficulty with our theory, in which MJO-related variations are forced in MLT winds through gravity-wave and tidal coupling, is that the intraseasonal peaks in Fig. 4 differ somewhat from those observed in the lower atmosphere. The MJO peak in the troposphere is broad: it was originally named the 40–50 day oscillation by Madden and Julian (1971), although later studies have often referred to it as the 30–60 day oscillation to stress the variable and broadband nature of the peak (see the review of Madden and Julian (1994)). In contrast, the peaks observed in Fig. 4 are sharper, and are displaced somewhat from the mean MJO peak at $\sim$45 days.

The band B peaks at 35–40 days seem to relate most easily with the 30–60 day MJO, whereas the stronger quasi-60 day peak that we observe in band A is at the long-period limit of MJO-related variability. However, the activity within bands A and B seems to occur at similar times (e.g., Fig. 5), suggesting that the two bands are closely related. Despite considerable interannual variability, the mean seasonal cycles of activity within bands A and B showed a tendency for an annual cycle, with greatest activity around January–February and least activity during August (Fig. 7). This is similar to both the interannual variability and mean annual variation of the MJO (see e.g., Madden, 1986; Hartmann and Gross, 1988; Gutzler and Madden, 1989), and is consistent with the hypothesized MJO-modulated tidal and gravity-wave driving of the oscillations within bands A and B.

Some clues as to how the MJO at $\sim$45 days might drive MLT oscillations of $\sim$60 days (band A) and

35–40 days (band B) is provided by the periodicities evident in the gravity-wave variances (Fig. 12). At 86–90 km there is a zonal peak at ~60 days, whereas at 92–98 km the zonal peak has shifted to ~45 days, and peaks in meridional velocity variance now appear at ~45 days, ~60 days, and ~90 days. We postulated that intraseasonal variations in upper-level meridional gravity-wave activity arose on interacting with the background flow below 90 km. Below 90 km, in addition to strong quasi-60 day wind variations (of frequency ω_{60}). there is of course a strong MLTSAO variation of ~183 days (frequency ω_{SAO}). Thus, gravity waves interacting nonlinearly with these two flow periodicities will yield a time series of gravity-wave variance containing not only the frequencies ω_{60} and ω_{SAO}, but also the interactive combinations $\omega_{60} \pm \omega_{SAO}$ These two combinations give rise to periods of ~90 days and ~45 days, which are very close to the peaks observed in Fig. 12b.

A logical extension of this argument may explain how the band A and B peaks are produced by wave forcing over MJO-related time scales. Since the MJO is centered at a period of ~45 days (frequency ω_{MJO}), it will presumably produce a similar period in convectively generated gravity-wave activity. Gravity waves are believed to play a major role in driving the SSAO (e.g., Sassi *et al*., 1993; Eckermann *et al*., 1995). Thus, when this MJO-modulated gravity-wave activity interacts with the upper stratospheric flow in forcing the SSAO, the emergent gravity-wave activity might be expected to contain frequencies $\omega_{MJO} \pm \omega_{SAO}$. These combinations yield periods of ~60 days and ~36 days, which are very similar to the band A and band B peaks detected in the MLT wind oscillations (Fig. 4) and gravity-wave variances (Fig. 12a). Similar effects may also influence diurnal tidal activity, and may explain the 60 day and strong 40 day peaks in this activity observed in Fig. 13.

The observed peaks in the zonal velocity spectra within the 20–25 day range (band C) seem to relate to the 20–25 day tropical tropospheric oscillation observed in the western Pacific region. This oscillation is known to induce similar periodicities in regional convective activity (Hartmann *et al*., 1992; Kiladis *et al*., 1994), and thus (presumably) in the intensity of convectively generated gravity waves and nonmigrating diurnal tides entering the middle atmosphere. Hartmann *et al*. (1992) noted that 20–25 day TTIV was most active during September–December, which again is very similar to the seasonal variations of band C activity observed in Fig. 7. This too is consistent with a forcing of the band C activity by convectively generated tides and gravity waves. Forcing by the diurnal tide seems to be most relevant to the band C activity, since there is a strong 24 day peak in diurnal tidal activity (see Fig. 13).

SUMMARY

Our analysis of over five years of horizontal velocity measurements of the MLT region over Christmas Island has revealed intraseasonal variations in the zonal winds, as initially reported by Eckermann and Vincent (1994). In this study, we have also found clear intraseasonal variations in the meridional winds, gravity-wave activity, and diurnal tidal amplitudes, all of which have similar periods to those initially detected in the zonal winds.

Three main period bands of activity in the zonal winds were identified, at around 60 days (band A), ~40 days (band B), and ~25 days (band C). The 60 day signal was also observed strongly in gravity-wave activity, and moderately in meridional wind and diurnal tidal activity. A 35 day signal was observed in meridional winds, and weak 40 day and 25 day peaks in gravity-wave activity were observed at 86–90 km. However, diurnal tidal amplitudes exhibited strong peaks at ~40 days and ~25 days throughout the 86–98 km height range. Periodicities in gravity-wave activity also exhibited height variations which may be due to nonlinear coupling with the background flow.

The activity in all three intraseasonal bands was associated with intraseasonal oscillations of the tropical troposphere. The peaks within bands A and B were within the range of the 30–60 day Madden–Julian Oscillation, and the mean annual variation of activity in bands A and B was similar to that observed for the MJO. Band C activity exhibited a period range and mean seasonal variation that agreed well with 20–25 day oscillations encountered in the tropical troposphere.

Our observations led us to propose that 30–60 day, 20–25 day and diurnal variations in tropical tropospheric convection produce intraseasonal cycles in the intensity of gravity waves and nonmigrating diurnal tides entering the middle atmosphere. Theoretical assessments of such wave production indicated that intraseasonal variations in the wave-induced driving of the zonal MLT flow will result, which in turn will produce intraseasonal variations in the mean zonal winds, as observed. Our observation of similar periodicities in diurnal tidal and gravity-wave activity in the MLT region support this theory.

Further observations and modeling are required to understand the intraseasonal behavior of the equatorial MLT region better. For example, it is still unclear whether these intraseasonal wind disturbances

are mean-flow or planetary-wave phenomena. It is also unclear how coherent they might be around the equatorial belt: for example, we showed that the activity here seems to differ somewhat from intraseasonal winds observed near the stratopause over India (Ziemke and Stanford, 1991; Kumar and Jain, 1994). Analysis of data from UARS instruments may provide information on these and other questions that have arisen from our initial analyses of equatorial MLT wind data from the central Pacific.

Acknowledgements—This research was performed in part under contract number N00014-95-C-2152 of the Naval Research Laboratory. The operation of the Christmas Island MF radar is supported by the Australian Research Council. Many thanks to Mary Anderson at Computational Physics, Inc., for her administrative support and to Rolando Garcia for comments.

REFERENCES

Alexander M. J. 1996 A simulated spectrum of convectively-generated gravity waves: propagation from the tropopause to the mesopause and effects on the middle atmosphere. *J. geophys. Res.* **101,** 1571–1588.

Alexander M. J. and Pfister L. 1995 Gravity wave momentum flux in the lower stratosphere over convection. *J. geophys. Res.* **22,** 2029–2032.

Anyamba E. K. and Weare B. C. 1995 Temporal variability of the 40–50 day oscillation in tropical convection. *Int. J. Climatol.* **15,** 379–402.

Bacmeister J. T., Schoeberl M. R., Summers M. E., Rosenfeld J. R. and Zhu X. 1995 Descent of long-lived trace gases into the winter polar vortex. *J. geophys. Res.* **100,** 11,669–11,684.

Baines P. G. 1995 Topographic effects in stratified flows. Cambridge University Press, 482 pp.

Bergman J. W. and Salby M. L. 1994 Equatorial wave activity derived from fluctuations in observed convection. *J. atmos. Sci.* **51,** 3791–3806.

Brasseur G. 1993 The response of the middle atmosphere to long-term and short-term solar variability: a two-dimensional model. *J. geophys. Res.* **98,** 23,079–23,090.

Burrage M. D., Skinner W. R., Gell D. A., Hays P. B., Marshall A. R., Ortland D. A., Manson A. H., Franke S. J., Fritts D. C., Hoffman P., McLandress C., Niciejewski R., Schmidlin F. J., Shepherd G. G., Singer W., Tsuda T. and Vincent R. A. 1996 Validation of mesosphere and lower thermosphere winds from the high resolution Doppler imager on UARS. *J. geophys. Res.* **101,** 10,365–10,392.

Canziani P. O., Holton J. R., Fishbein E. and Froidevaux L. 1995 Equatorial Kelvin wave variability during 1992 and 1993. *J. geophys. Res.* **100,** 5193–5202.

Connor L. N. and Avery S. K. 1996 A three-year gravity wave climatology of the mesosphere and lower thermosphere over Kauai. *J. geophys. Res.* **101,** 4065–4077.

Dunkerton T. J. and Crum F. X. 1995 Eastward propagating ~2- to 15-day equatorial convection and its relation to the tropical intraseasonal oscillation. *J. geophys. Res.* **100,** 25,781–25,790.

Eckermann S. D. and C. J. Marks 1996 An idealized ray model of gravity wave-tidal interactions. *J. geophys. Res.* **101,** 21,195–21,212.

Eckermann S. D. and Vincent R. A. 1994 First observations of intraseasonal oscillations in the equatorial mesosphere and lower thermosphere. *Geophys. Res. Lett.* **21,** 265–268.

Eckermann S. D., Hirota I. and Hocking W. K. 1995 Gravity wave and equatorial wave morphology of the stratosphere derived from long-term rocket soundings. *Q. J. R. Meteorol. Soc.* **121,** 149–186.

Forbes J. M. and Leveroni S. 1992 Quasi 16-day oscillation in the ionosphere. *Geophys. Res. Lett.* **19,** 981–984.

Forbes J. M., Hagan M. E., Miyahara S., Vial F., Manson A. H., Meek C. E. and Portnyagin Y. I. 1995 Quasi 16-day oscillation in the mesosphere and lower thermosphere. *J. geophys. Res* **100,** 9149–9163.

Fritts D. C. and VanZandt T. E. 1993 Spectral estimates of gravity wave energy and momentum fluxes. Part I: Energy dissipation, acceleration, and constraints. *J. Atmos. Sci.* **50,** 3685–3694.

Garcia R. R., Dunkerton T. J., Lieberman R. and Vincent R.A. 1997 Climatology of the semiannual oscillation of the tropical middle atmosphere, *J. geophys. Res.* (in press).

Ghil M. and Mo K. 1991 Intraseasonal oscillations in the global atmosphere, Part I: Northern hemisphere and tropics. *J. atmos. Sci.* **48,** 752–779.

Gutzler D. S. and Madden R. A. 1989 Seasonal variations in the spatial structure of intraseasonal tropical wind fluctuations. *J. atmos. Sci.* **46,** 641–660.

Gutzler D. S., Kiladis G. N., Meehl G. A., Weickmann K. M. and Wheeler M. 1994 The global climate of December 1992–February 1993. Part II: Large-scale variability across the tropical western Pacific during TOGA COARE. *J. Clim.* **7,** 1606–1622.

Hamilton K. 1981 Latent heat release as a possible forcing mechanism for atmospheric tides. *Mon. Wea. Rev.* **109,** 3–17.

Hamilton K. 1995 Aspects of mesospheric simulation in a comprehensive general circulation model. In *The Upper Mesosphere and Lower Thermosphere: A Review of Experiment and Theory*, (Johnson R. M. and Killeen T. L. eds). AGU Geophysical Monograph Series, 87, pp. 255–264.

Harris T. J. and Vincent R. A. 1993 The quasi-two-day wave observed in the equatorial middle atmosphere. *J. geophys. Res.* **98,** 10,481–10,490.

Hartmann D. L. and Gross J. L. 1988 Seasonal variability of the 40–50 day oscillation in wind and rainfall in the tropics. *J. atmos. Sci.* **45,** 2680–2702.

Hartmann D. L., Michelson M. I. and Klein S. A. 1992 Seasonal variations of tropical intraseasonal oscillations: a 20–25-day oscillation in the western Pacific. *J. atmos. Sci.* **49,** 1277–1289.

Hayashi Y. and Golder D. G. 1993 Tropical 40–50- and 25–30-day oscillations appearing in realistic and idealized GFDL climate models and the ECMWF dataset. *J. atmos. Sci.* **50,** 464–494.

Held I. M., Helmer R. S. and Ramaswamy V. 1993 Radiative-convective equilibrium with explicit two-dimensional moist convection. *J. atmos. Sci.* **50,** 3909–3927.

Hendon H. H. and Salby M. L. 1994 The life cycle of the Madden-Julian oscillation. *J. atmos. Sci.* **51,** 2225–2237.

Hendon H. H. and Salby M. L. 1996 Planetary-scale circulations forced by intraseasonal variations of observed convection. *J. atmos. Sci.* **53,** 1751–1758.

Hendon H. H. and Woodberry K. 1993 The diurnal cycle of tropical convection. *J. geophys. Res.* **98,** 16623–16637.

Hirooka T. and Hirota I. 1989 Further evidence of normal mode Rossby waves. *Pure. Appl. Geophys.* **130,** 277–289.

Hirota I. 1978 Equatorial waves in the upper stratosphere and mesosphere in relation to the semiannual oscillation of the zonal wind. *J. atmos. Sci.* **35,** 714–722.

Holton J. R. 1984 The generation of mesospheric planetary waves by zonally asymmetric gravity wave breaking. *J. atmos. Sci.* **41,** 3427–3430.

Hood L. L., Huang Z. and Bougher S. W. 1991 Mesospheric effects of solar ultraviolet variations: Further analysis of SME IR ozone and Nimbus 7 SAMS temperature data. *J. geophys. Res.* **96,** 12,989–13,002.

Huang N. E., Long S. R., Tung C.-C., Donelan M. A., Yuan Y. and Lai R. J. 1992 The local properties of ocean surface waves using the phase-time method. *Geophys. Res. Lett.* **19,** 685–688.

Isler J. R. and Fritts D. C. 1996 Gravity wave variability and interaction with lower-frequency motions in the mesosphere and lower thermosphere. *J. atmos. Sci.* **53,** 37–48.

Karoly D. J., Roff G. L. and Reeder M. J. 1996 Gravity wave activity associated with tropical convection detected in TOGA COARE sounding data. *Geophys. Res. Lett.* **23,** 261–264.

Kiladis G. N. and Wheeler M. 1995 Horizontal and vertical structure of observed tropospheric equatorial Rossby waves. *J. geophys. Res.* **100,** 22,981–22,997.

Kiladis G. N., Meehl G. A. and Weickmann K. M. 1994 Large-scale circulation associated with westerly wind bursts and deep convection over the western equatorial Pacific. *J. geophys. Res.* **99,** 18,527–18,544.

Kumar K. and Jain A. R. 1994 Latitudinal variations of 30–70 day period waves over the tropical Indian zone. *J. atmos. terr. Phys.* **56,** 1135–1145.

Lieberman R. S. 1991 Nonmigrating diurnal tides in the equatorial middle atmosphere. *J. atmos. Sci.* **48,** 1112–1123.

Lieberman R. S. and Leovy C. B. 1995 A numerical model of nonmigrating diurnal tides between the surface and 65 km. *J. atmos. Sci.* **52,** 389–409.

Lieberman R. S., Burrage M. D., Gell D. A., Hays P. B., Marshall A. R., Ortland D. A., Skinner W. R., Wu D. L., Vincent R. A. and Franke S. J. 1993 Zonal mean winds in the equatorial mesosphere and lower thermosphere observed by the high resolution Doppler imager. *Geophys. Res. Lett.* **20,** 2849–2852.

Madden R. A. 1986 Seasonal variations of the 40–50 day oscillation. *J. atmos. Sci.* **43,** 3138–3158.

Madden R. A. and Julian P. R. 1971 Detection of a 40–50 day oscillation in the zonal wind in the tropical Pacific. *J. atmos. Sci.* **28,** 702–708.

Madden R. A. and Julian P. R. 1972 Description of global-scale circulation cells in the tropics with a 40–50 day period. *J. atmos. Sci.* **29,** 1109–1123.

Madden R. A. and Julian P. R. 1994 Observations of the 40–50-day tropical oscillation—A review. *Mon. Wea. Rev.* **122,** 814–837.

McLandress C. and McFarlane N. A. 1993 Interactions between orographic gravity waves and forced stationary planetary waves in the winter northern hemisphere middle atmosphere. *J. atmos. Sci.* **50,** 1966–1990.

McLandress C., Shepherd G. G. and Solheim B. H. 1996 Satellite observations of thermospheric tides: Results from the Wind Imaging Interferometer on UARS. *J. geophys. Res.* **101,** 4093–4114.

Nagpal O. P. and Raghavarao R. 1991 On the wave forcing of the semi-annual zonal wind oscillation. *J. atmos. terr. Phys.* **53,** 1181–1193.

Nagpal O. P., Dhaka S. K. and Srivastav S. K. 1994 Wave characteristics in the troposphere and stratosphere over the Indian tropics during the DYANA campaign. *J. atmos. terr. Phys.* **56,** 1117–1133.

Nakamura T., Fritts D. C., Isler J. R., Reid I.M., Tsuda T. and Vincent R. A. 1997 Short-period fluctuations of the diurnal tide observed with low-latitude MF and meteor radars during CADRE: evidence for gravity wave/tidal interactions, *J. geophys. Res.* (in press).

Palo S. E. and Avery S. K. 1993 Mean winds and the semiannual oscillation in the mesosphere and lower thermosphere at Christmas Island. *J. geophys. Res.* **98,** 20,385–20,400.

Palo S. E. and Avery S. K. 1996 Observations of the quasi-two-day wave in the middle and lower atmosphere over Christmas Island. *J. geophys. Res.* **101,** 12833–12846.

Parker D. E. 1973 Equatorial Kelvin waves at 100 millibars. *Q. J. R. Meteorol. Soc.* **99,** 116–120.

Parish H. F., J. M. Forbes and F. Kamalabadi 1995 Analysis of wave signatures in the equatorial ionosphere. In *The Upper Mesosphere and Thermosphere: A Review of Experiment and Theory* (Johnson R. M. and Killeen T. L. eds). AGU Geographical Monograph Series, 87, pp. 111–119.

Pfister L., Scott S., Loewenstein M., Bowen S. and Legg M. 1993a Mesoscale disturbances in the tropical stratosphere excited by convection: observations and effects on the stratospheric momentum budget. *J. atmos. Sci.* **50,** 1058–1075.

Pfister L., Chan K. R., Bui T. P., Bowen S., Legg M., Gary B., Kelly K., Proffitt M. and Starr W. 1993b Gravity waves generated by a tropical cyclone during the STEP tropical field program: a case study. *J. geophys. Res.* **98,** 8611–8638.

Rastogi P. K., Kudeki E. and Sürücü F. 1996 Distortion of gravity wave spectra of horizontal winds measured in atmospheric radar experiments. *Radio Sci.* **31,** 105–118.

Salby M. L. and Hendon H. H. 1994 Intraseasonal behavior of clouds, temperature and motion in the tropics. *J. atmos. Sci.* **51,** 2207–2224.

Salby M. L., Garcia R. R. and Hendon H. H. 1994 Planetary-scale circulations in the presence of climatological and wave-induced heating. *J. atmos. Sci.* **51,** 2344–2367.

Sassi F., Garcia R. R. and Boville B. A. 1993 The stratopause semiannual oscillation in the NCAR community climate model. *J. atmos. Sci.* **50,** 3608–3624.

Sheu R.-S. and Liu G. 1995 Atmospheric humidity variations associated with westerly wind bursts during Tropical Ocean Global Atmosphere (TOGA) Coupled Ocean Atmosphere Response Experiment (COARE). *J. geophys. Res.* **100,** 25,759–25,768.

Smith A. K. 1996 Longitudinal variations in mesospheric winds: Evidence for gravity wave filtering by planetary waves. *J. atmos. Sci.* **53,** 1156–1173.

Stening R. J., Manson A. H., Meek C. E. and Vincent R. A. 1994 Lunar tidal winds at Adelaide and Saskatoon at 80 to 100 km heights: 1985–1990. *J. geophys. Res.* **99,** 13,273–13,280.

Stening, R. J., Schlapp D.M. and Vincent R.A. 1997 Lunar tides in the mesosphere over Christmas Island (2°N, 203°E). *J. geophys. Res.* (submitted).

Summers M. E., Strobel D. F., Bevilacqua R. M., Zhu X., Deland M. T., Allen M. and Keating G. M. 1990 A model study of the response of mesospheric ozone to short-term solar ultraviolet flux variations. *J. geophys. Res.* **95,** 22,523–22,538.

Vincent R. A. 1993 Long-period motions in the equatorial mesosphere. *J. atmos. terr. Phys.* **55,** 1067–1080.

Vincent R. A. and Eckermann S. D. 1990 VHF radar observations of mesoscale motins in the troposphere: Evidence for gravity-wave Doppler shifting. *Radio Sci.* **25,** 1019–1037.

Vincent R. A. and Lesicar D. 1991 Dynamics of the equatorial mesosphere: First results with a new generation partial reflection radar. *Geophys. Res. Lett.* **18,** 825–828.

Williams C. R. and Avery S. K. 1992 Analysis of long-period waves using the mesosphere-stratosphere-troposphere radar at Poker Flat, Alaska. *J. geophys. Res.* **97,** pp. 20,855–20,861.

Williams C. R. and Avery S. K. 1996 Diurnal nonmigrating tidal oscillations forced by deep convective clouds. *J. geophys. Res.* **101,** 4079–4091.

Wu D. L., Hays P. B., Skinner W. R., Marshall A. R., Burrage M. D., Lieberman R. S. and Ortland D. A. 1993 Observations of the quasi 2-day wave from the high resolution Doppler imager on UARS. *Geophys. Res. Lett.* **20,** 2853–2856.

Ziemke J. R. and Stanford J. L. 1991 One-to-two month oscillations: Observed high-latitude tropospheric and stratospheric response to tropical forcing. *J. atmos. Sci.* **48,** 1336–1347.